DIFFRACTIVE DISSOCIATION OF HADRONS*

By H. J. Lubatti**

Department of Physics, University of Washington, Seattle***

(Presented at the XII Cracow School of Theoretical Physics, Zakopane, June 8–18, 1972)

Diffractive dissociation of pions, kaons and nucleons is reviewed, and the data are compared with elastic scattering. Similarities in the final states are stressed, and the important role of off-mass-shell π-hadron scattering in diffractive dissociation is emphasized. Several new experimental techniques employed in the study of diffractive processes are discussed.

1. Introduction

During the past decade we have had the pleasure of accumulating considerable experimental information about the strong interactions. First there was the pioneering work of the bubble chambers which allowed one to establish the spectrum of the excited hadronic states. Then, having the knowledge of the richness of the hadronic spectrum, many clever and difficult experiments were performed which were directed at studying the dependence of the strong interactions on energy, momentum transfer, and internal and external quantum numbers. These experiments continue and each year we have more detailed information about specific interactions. In addition to the study of specific channels (exclusive reactions) there has always been experimental work on the study of the momentum and energy dependence of the secondaries emitted when two hadrons collide. In fact, some of the earliest experimental work of this type was performed by the Cracow and Warsaw groups. More recently such experimental studies have become extremely popular, and in the past three years an enormous amount of data on these so-called inclusive reactions has beceme available.

From these data certain trends are becoming apparent. For example, the data on exclusive reactions have shown certain common features such as:

(*i*) the peripheral nature of the strong interactions

(*ii*) the decrease of production cross-sections with energy according to $1/p^n$, where n

* Work supported in part by NSF Science development grant GU-2655.

** A. P. Sloan Foundation Fellow.

*** Address: Visual Techniques Laboratory, Department of Physics, University of Washington, Seattle, Washington 98195, USA.

is related to the quantum numbers exchanged in the t-channel, and p is the momentum of the incident particle in the laboratory.

(*iii*) Elastic and total cross-sections are approximately energy independent.

These and other common features have led to the belief that the singularities in the t-channel (u-channel) determine the behaviour of the observed cross-sections in the s-channel for small t (u). The usual description these days is in terms of the exchange of Regge trajectories in the t or u-channel.

The Regge model has had some difficulty in coping with total and elastic cross-sections in that the Pomeranchuk trajectory which is used for describing constant cross-section processes appears to have a smaller slope than the other empirically determined trajectories such as those of the ϱ and A. In addition, it has not been possible to associate resonant states with the Pomeranchuk trajectory.

It is curious that these difficulties are associated with elastic cross-sections which seem to be geometrical in nature; *i.e.*, we believe that we can understand such processes in terms of our usual notions of diffraction by an absorbing target. Such a wave mechanical (geometrical) description of elastic scattering can be extended easily to particle production. This was first proposed by Feinberg and Pomeranchuk in 1953, applied by Glauber to deuterium stripping and discussed by Good and Walker in 1960 with regard to hadronic processes and recently refined by Białas, Czyż and Kotański [1]. The basic ideas are similar to the $|K_S\rangle$ regeneration from a $|K_L\rangle$ beam which results from the differential absorption of K and $\bar{K}$ in nuclear matter.

The basic notions of diffractive dissociation have never been precisely defined but rather they have been developed by analogy to our intuitive geometrical ideas of diffractive elastic scattering. The explanation of diffractive scattering in terms of t-channel exchanges leads to the concept of vacuum exchange or in the Regge language the exchange of the Pomeranchuk trajectory, and this latter quantity also is not well defined.

Such a situation presents a challenge to the author since he is proposing to discuss the status of the existing experimental information on diffractive dissociation and finds that it is difficult to define unambiguously such a process.

The plan which will be followed is first to remind the reader of some of the salient features of elastic scattering and then to look at some inelastic reactions initiated by incident π, K, p, and their antiparticles and see to what extent there exist processes which are similar to elastic scattering. Data from both nucleon and nuclear targets will be discussed.

2. *Elastic scattering*

Elastic and total cross-sections are among the best studied strong interactions, and, as is well known, the two processes are related by the optical theorem which states that the total cross-section is proportional to the imaginary part of the forward scattering amplitude.

The general picture which has emerged is that elastic scattering is a diffractive process, by which we mean that the angular distribution behaves as though the target were an absorbing disk which removes part of the wave front. The result is the usual diffraction

pattern which is well known from classical optics. This geometrical interpretation is supported by the fact that the integrated elastic cross-section is practically energy independent. Total cross-sections also seem to be energy independent. There is also the additional point that s-channel helicity seems to be conserved in elastic scattering processes [2].

Such a geometrical process which does not allow for the change of internal quantum numbers (C, G, T, Y, B, $\sigma = P(-1)^J$) seems almost impossible to reconcile with the usual ideas of particle exchange in the crossed channel. In order to use the t-channel language one has been lead to the notion of the exchange of a Pomeron which carries the quantum numbers of the vaccum ($Y = B = T = 0$; G, C and σ even).

The simple geometrical interpretation of no exchange of quantum numbers is somewhat clouded by the experimental observation that polarization is non zero in elastic scattering processes. Polarization requires some non Pomeron process which can interfere with the Pomeron amplitude. Another phenomenon which demonstrates that there must be some quantum number exchange contributing is the so-called cross over effect. This results when differential cross-sections for particles and antiparticles are compared. The effect, which is shown for Kp elastic scattering in Figure 1, is that the antiparticle (K^-) cross-sec-

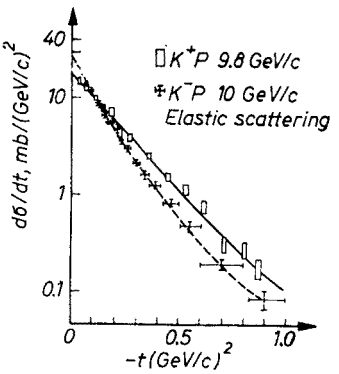

Fig. 1. Cross over effect in Kp elastic scattering at 10 GeV/c (Ref. [3])

tion is larger than the particle (K^+) cross-section at $t = 0$ but falls more rapidly with increasing t. At $|t| \simeq 0.15$ (GeV/c)^2 the two cross-sections become equal; for $|t| > 0.15$ the particle cross-section exceeds the antiparticle cross-section.

To summarize, the salient features of elastic scattering are:

(*i*) Sharp forward peaking of $d\sigma/dt$ which reflects the size of the target.
(*ii*) The integrated cross-section is approximately constant.
(*iii*) s-channel helicity is conserved.
(*iv*) Existence of the cross over effect.
(*v*) Existence of polarization.
(*vi*) The internal quantum numbers of the scattered particles do not change.

With these points in mind some inelastic reactions will be examined to see to what extent reactions which are similar to the elastic scattering can be found. The data which

are available consist of dissociation reactions involving π, K, and N (both particle and antiparticle). If internal quantum numbers are conserved one would expect dissociation into the following final states:

(*i*) $\pi \to 3\pi, 5\pi, \ldots$?

(*ii*) $K \to K\pi\pi, K\pi\pi\pi, \ldots$?

(*iii*) $N \to N\pi, N\pi\pi, \ldots$?

where the final states may or may not be established resonances.

Before beginning to look at the data there will be a discussion of the experimental techniques which are used for the study of diffractive dissociation, and a brief review of some kinematic notions.

3. Experimental techniques

Experiments on diffractive dissociation have employed most of the experimental techniques which are available. Both nucleon and nuclear targets have been used. Some of the first experiments were done with emulsions, which, because of their excellent spatial resolution, allow one to study in detail the production vertex, and, hence, detect very slow protons (boil-off protons). This technique is excellent for rejecting interactions in which the nucleus breaks-up. However, emulsion experiments are usually low statistics experiments, with few kinematic constraints, and even though recently there has been some very interesting work at Serpukhov using emulsions, [4] this technique will not be considered further. Most of the existing experiments have been done with bubble chambers. Heavy liquid bubble chambers, hydrogen, neon-hydrogen mixtures, and deuterium-filled chambers have been used to study coherent production of unstable particles. Electronic techniques using optical and wire chambers have most recently been used, and these have resulted in high statistics experiments.

Several new ideas are being examined. One involves using a solid state detector as a target and then as a detector of the recoiling nucleus. Another is to use a bubble chamber which is triggered by information obtained from wire chamber spectrometers. A third is to use a streamer chamber in which the gas of the chamber (helium) is used as the target and then the streamer chamber becomes a detector of the recoiling helium nucleus. These new techniques are discussed in some detail in Section 8.

3.1. Kinematics

This paper shall be concerned with the reaction $X+\mathcal{N} \to Y+\mathcal{N}$ (see Figure 2), where $\mathcal{N}$ represents the target. A requirement for diffractive dissociation is that the momentum transfer to the target be small relative to the incident momentum. If this condition is satisfied, it is simple to show that the minimum three momentum transfer required for energy conservation is given by

$$q_L \simeq \frac{M_Y^2 - M_X^2}{2P_X^{\text{in}}}, \tag{3.1}$$

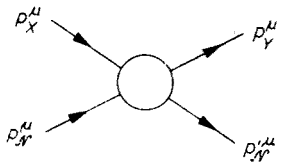

Fig. 2. Two body process

where the subscript L indicates that the minimum momentum transfer is along the beam (*i.e.*, longitudinal). This can be demonstrated easily by considering the four-momentum transfer

$$t \equiv (P_X^\mu - P_Y^\mu)^2 = M_X^2 + M_Y^2 - 2E_X E_Y + 2P_X P_Y \cos\theta, \tag{3.2}$$

where θ is the laboratory angle between particle Y and the beam. Hence, for $\cos\theta = 1$

$$t_{\min} = -(E_X - E_Y)^2 + (P_X - P_Y)^2 \simeq (q_L)^2; \tag{3.3}$$

a new variable can be defined

$$t' \equiv |t| - |t|_{\min} = 2P_X P_Y(1 - \cos\theta) \tag{3.4}$$

which for small θ gives

$$t' \simeq P_X P_Y \theta^2 = \frac{P_X}{P_Y}(q_T)^2, \tag{3.5}$$

where q_T is the momentum which is transverse to the beam. Many of the results which have been published on nuclear targets make the approximations

$$t' \simeq q_T^2, \qquad |t|_{\min} \simeq q_L^2. \tag{3.6}$$

Such approximations become less reliable at incident momenta where $P_X/P_Y > 1$.

Longitudinal rapidity is another quantity which can be useful in discussing diffractive dissociation. It is defined by the following relation

$$P_L^Y = [(P_T^Y)^2 + m_Y^2]^{\frac{1}{2}} \sinh y, \tag{3.7}$$

where the subscripts L and T refer to longitudinal and transverse components of momentum.

In general

$$P_X^\mu = m_X(\cosh y_X, 0, 0, \sinh y_X) \tag{3.8}$$

$$P_{\mathcal{N}} = m_{\mathcal{N}}(\cosh y_{\mathcal{N}}, 0, 0, \sinh y_{\mathcal{N}}) \tag{3.9}$$

$$P_Y = m'_Y\left(\cosh y, \frac{q_X}{m'_Y}, \frac{q_y}{m'_Y}, \sinh y\right) \tag{3.10}$$

$$m'_Y = (m_Y^2 + |q|^2)^{\frac{1}{2}}, \qquad \vec{q} = \vec{P}_T^Y \tag{3.11}$$

$$P_X^\mu \cdot P_{\mathcal{N}}^\mu = m_X m_{\mathcal{N}} \cosh(y_{\mathcal{N}} - y_X) \tag{3.12}$$

$$P_X^\mu \cdot P_Y^\mu = m_X m_Y' \cosh(y - y_X) \tag{3.13}$$

$$P_{\mathcal{N}}^\mu + P_Y^\mu = m_{\mathcal{N}} m_Y' \cosh(y_{\mathcal{N}} - y). \tag{3.14}$$

A good approximation for equal mass particles is

$$y_{\mathcal{N}} - y_X \simeq \ln\left(\frac{2E_X}{m_X}\right) \tag{3.15}$$

which gives the rapidity gap between target and projectile. For a 30 GeV/c proton one has approximately 4 units of rapidity separating the target and projectile.

Diffractive dissociation can be defined in terms of processes for which there exist large gaps in the rapidity distribution of the final state particles. Intuitively, large gaps in rapidity mean that the two processes shown in Figure 3 do not communicate any information. In a multiperipheral model this means Pomeron coupling.

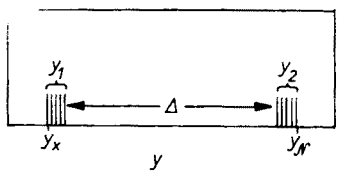

Fig. 3. Longitudinal rapidity plot illustrating the large gaps expected in diffractive processes

For single diffractive dissociation we expect only one cluster of particles in y-space. If we take dissociation of particle X we expect in such a case $y_1 - y_X \simeq 0$ while $y_1 - y_{\mathcal{N}} \simeq$ $\simeq y_X - y_{\mathcal{N}}$; as a result the spread of y_1 must be much smaller than $y_X - y_{\mathcal{N}}$ (y_1 is defined in Figure 3).

3.2. Nuclear targets

An experimental technique which has been very useful in the study of diffractive dissociation has been to use nuclear targets. In these experiments one looks for interactions in which energetic particles dissociate and the nucleus recoils in its ground state. These are called coherent processes.

In order to mathematically describe such interactions one must sum amplitudes from interactions on each nucleon in the nucleus. The reader can easily verify that the result is a suppression of spin and isotopic spin couplings and enhancement of scalar couplings [5]. In the Regge model this implies selecting reactions which are eventually dominated by Pomeron exchange. Note, however, that it is possible to have a coherent process in which internal quantum numbers are exchanged. This involves all of the isoscalar, non-spin couplings which one can make in the t-channel. An example is ω (φ) exchange. Note that η and η' exchange are suppressed because they require spin flip at the nucleon anti-nucleon vertex.

A consequence of selecting scalar couplings and small four momentum transfer is that for coherent processes involving π and K (in general $J^P = 0^-$) incident particles, the dissociated system will be in a spin parity state such that $P = (-1)^{J+1}$ [5]. No such rule

holds for dissociating Fermions; however, Morrison has conjectured that all diffractive dissociation reactions obey the rule $\Delta P = (-1)^{\Delta J}$ [6]. This conjecture has not been experimentally verified for nucleon dissociation — the only reaction for which it is not a trivial consequence of angular momentum conservation.

In coherent processes the momentum transfer distributions are limited by the dimension of the nucleus. The general result is that the width of the diffraction pattern is inversely proportional to the radius of the nucleus. For a light nucleus this results in $t' \leqslant 0.03$ $(\mathrm{GeV}/c)^2$. A more precise statement is that such processes give momentum transfer distributions which are governed by the nuclear form factor, which is simply the Fourier transform of the nuclear matter distribution. It is well known that rescattering corrections and absorption of the incident particle complicate this simple picture. It is just this complication which allows for the interesting possibility of being able to obtain unstable particle nucleon cross-sections from these coherent interactions on nuclei. Note that the limitation to small t' means that data from nuclear targets can give little or no information on the question of helicity conservation.

An experimental disadvantage in using nuclear targets is that the fast particles in the laboratory must be measured precisely, since the momentum of the recoiling nucleus is practically impossible to measure. A typical recoil momentum of a light nucleus is less than 150 MeV/c (less than 50 MeV/c for a Pb nucleus). Such low momenta particles which have large Z have ranges of a few microns. The results is that measurements by the usual experimental techniques are extremely difficult.

The best way to avoid such difficulties is to use targets which are also detectors. Solid state detectors and streamer chambers filled with He gas give the possibility of making measurements on the recoil nucleus. These techniques will be discussed in Section 8.

In the experiments where the nuclear recoil is not directly observed, it is not possible to unambiguously separate the coherent and incoherent events. The typical momentum transfer distribution which is observed is sketched in Figure 4. The usual procedure for

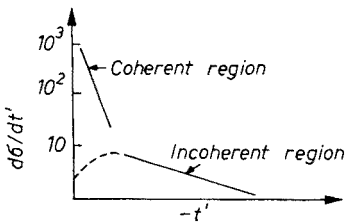

Fig. 4. Typical momentum transfer dependence when the target is a nucleus. Dotted line shows behaviour of incoherent cross-section as $t' \to 0$

obtaining cross-sections is to assume two analytic functions and fit them to the t' distribution. From the Pauli principle we would expect that $d\sigma/dt$ for the incoherent events would go to zero at $t = 0$; However, rescattering (or absorption) allows for some incoherent production at $t = 0$. The error in normalization introduced by this uncertainly is usually small since the ratio of coherent to incoherent events is usually one to two orders of magnitude.

3.3. Nucleon targets

Nucleon targets have been used extensively in the study of diffractive dissociation. Because the nucleon can be given considerable momentum it is possible to study the dissociation of the incident particle by performing missing mass experiments in which the momentum and angle of the recoiling nucleon are determined in a spectrometer. It is also possible to study the dissociation of the target nucleon into particles which have relatively low momenta in the laboratory, with small momentum transfer to the incident particle. In this case two types of experiments are possible: (*i*) A missing mass experiment in which the angle and momentum of the recoiling incident particle are measured in a single arm spectrometer. (*ii*) The measurement of the fast and slow particles in the laboratory. This requires that the apparatus cover a large solid angle and be capable of making measurements over a large range of momenta.

The missing mass experiments take all interactions and look for structure in the missing mass spectrum; as a result, only cross-sections and momentum transfer distributions are obtained. In addition, these experiments often have difficulties in absolute normalization. They also have a lower limit in t. For projectile dissociation this results from protons stopping in the target or target walls. For target dissociation it is a result of requiring that the projectile be scattered out of the beam.

In general the separation of diffractive dissociation from the usual production processes is complicated when the target is a nucleon. Recently, several bubble chamber groups have been using the techniques of longitudinal phase space analysis [7], and this seems to give relatively "clean" samples of single diffractive dissociation. These results will be discussed below. As the energy of the incident particle increases (particularly at NAL energies) the difficulty in separating such processes will decrease.

4. Pion dissociation

Experiments have been performed up to 16 GeV/c incident pion momentum in bubble chambers and more recently with the CERN spectrometer facility. To date the pion has not been observed to dissociate into more than five pions. This limitation on multiplicity may result from the large mass of the high multiplicity pion states, *i.e.*, the form factor of the target suppresses the reaction because the minimum momentum transfer is too large.

4.1. Nuclear targets ($\pi \to 3\pi$)

A number of experiments have been performed. The earliest experiments, at several energies, were performed with heavy liquid bubble chambers. Recently there has been a high statistics counter experiment.

The t' distribution for neutral and charged final states from the experiments of Allard *et al.* [8] and Daugeras *et.al.* [9] are given in Figures 5a, b. A more recent experiment at Dubna [10] using a 5 GeV/c π^- beam in a bubble chamber filled with Propane gives the t' distribution obtained in Figure 5c. A recent high statistics counter experiment

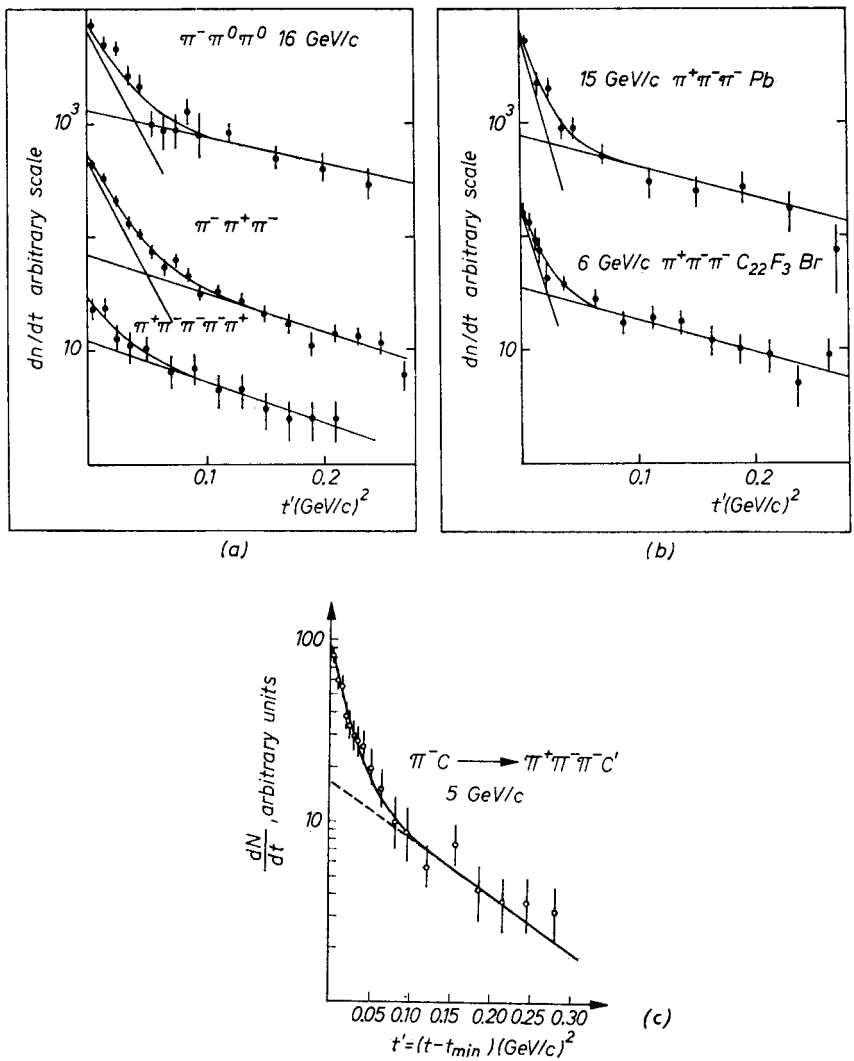

Fig. 5. Typical t' distribution obtained for three pion production in heavy liquid bubble chambers: a) Chamber filled with C_2F_5Cl (Ref. [8, 9]); b) Pb target inserted in HLBC for 15 GeV/c run (Ref. [8]); c) Chamber filled with Propane (Ref. [10])

at CERN [11] using 15 GeV/c pions[1] has given the results shown in Figure 6. In each of the above experiments one observes a t' distribution with a forward peak which corresponds to the form factor of the nuclear target. The resolution of the bubble chamber is clearly not as good as that of the CERN spectrometer, but in each case when one corrects the t' distribution for instrumental resolution one obtains an exponential distribution for $d\sigma/dt'$ with a slope parameter which agrees with the particular nuclear radius involved in the

[1] See the presentation of Dr Beusch, *Acta Phys. Polon.*, **B3**, 679 (1972).

process. Therefore, one concludes that he is observing a coherent process in which the nucleus recoils intact. The large t' tail has a slope of approximately 8 $(\mathrm{GeV}/c)^{-2}$, which is typical of interactions on a single nucleon. These large t' events presumably are production processes in which nuclear break-up occurs.

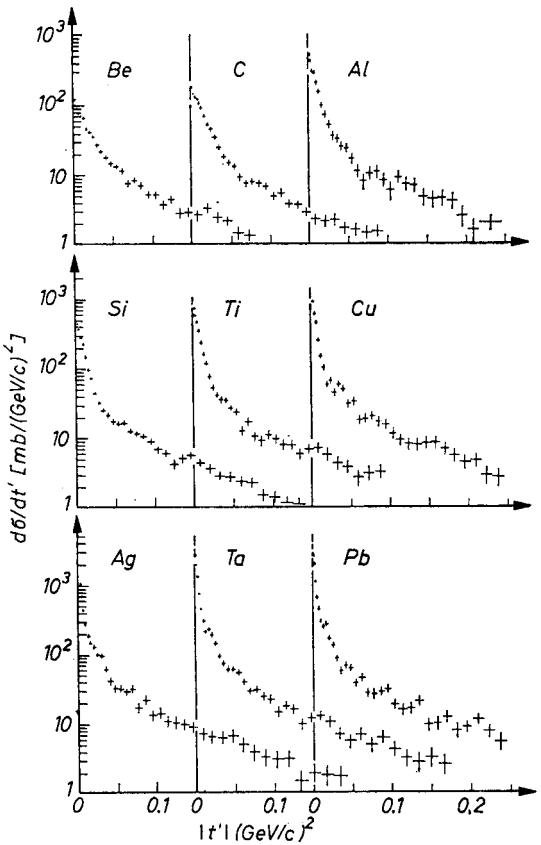

Fig. 6. t' distribution for a range of nuclei (Ref. [11])

The three pion mass distribution obtained by these experiments is shown in Figure 7. In each case the sample of coherent nuclear interactions has been enhanced by choosing only events with small t'. It must be noted that although the threshold for three pions is 0.42 GeV, the coherent production from nuclei gives a three pion mass spectrum which begins at approximately 0.9 GeV, peaks at 1.1 GeV, and falls to one-half its peak value at approximately 1.3 GeV. This enhancement is usually called the A_1. The two body mass distributions which are given in Figures 8a, b, c show that the A_1 consists mainly of $\varrho\pi$. A study of the angular distributions for the bubble chamber data in the region $0.9 < m(3\pi) < 1.2$ GeV indicates that the $\varrho\pi$ system is predominantly 1^+ s-wave. The CERN experimenters are currently performing their angular analysis and Dr Beusch will discuss their conclusions.

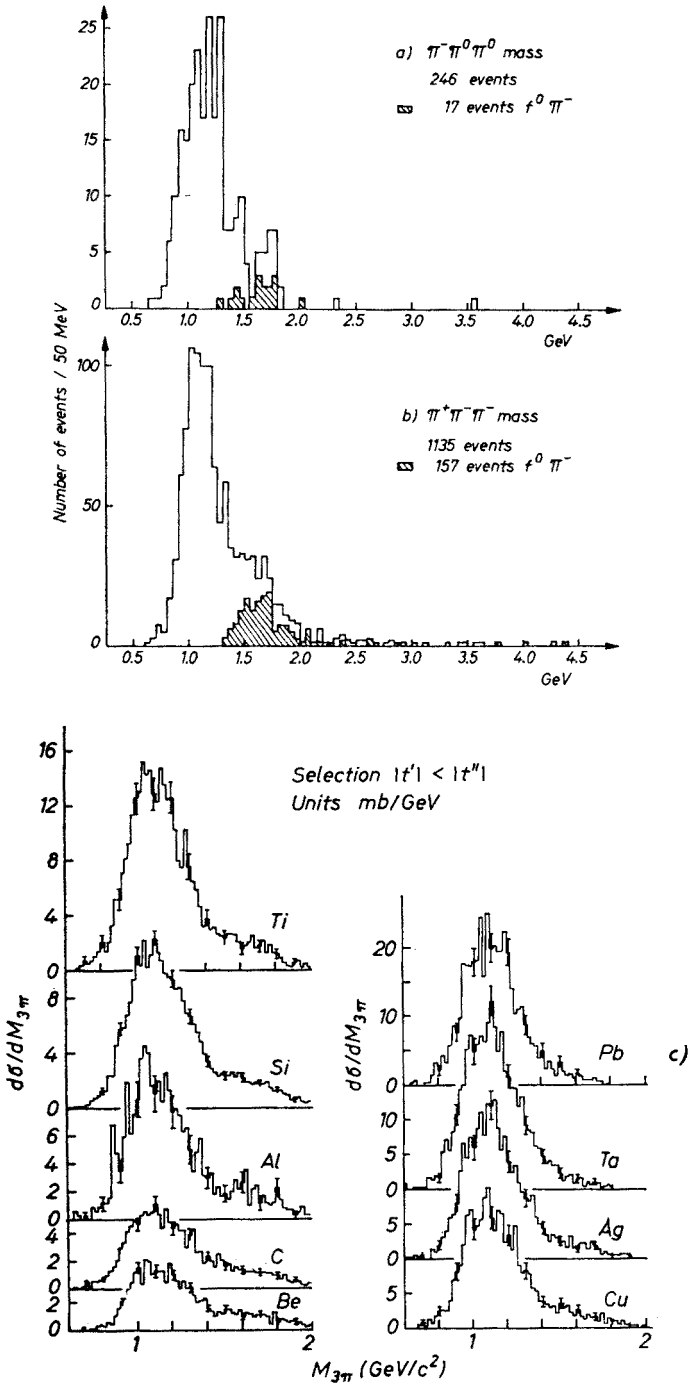

Fig. 7.a) $\pi^-2\pi^0$ effective mass distribution for coherent events (Ref. [9]); b) $\pi^+2\pi^-$ effective mass distribution for coherent events (Ref. [8]); c) $M(\pi^+2\pi^-)$ effective mass distribution for coherent events from several targets (Ref. [11])

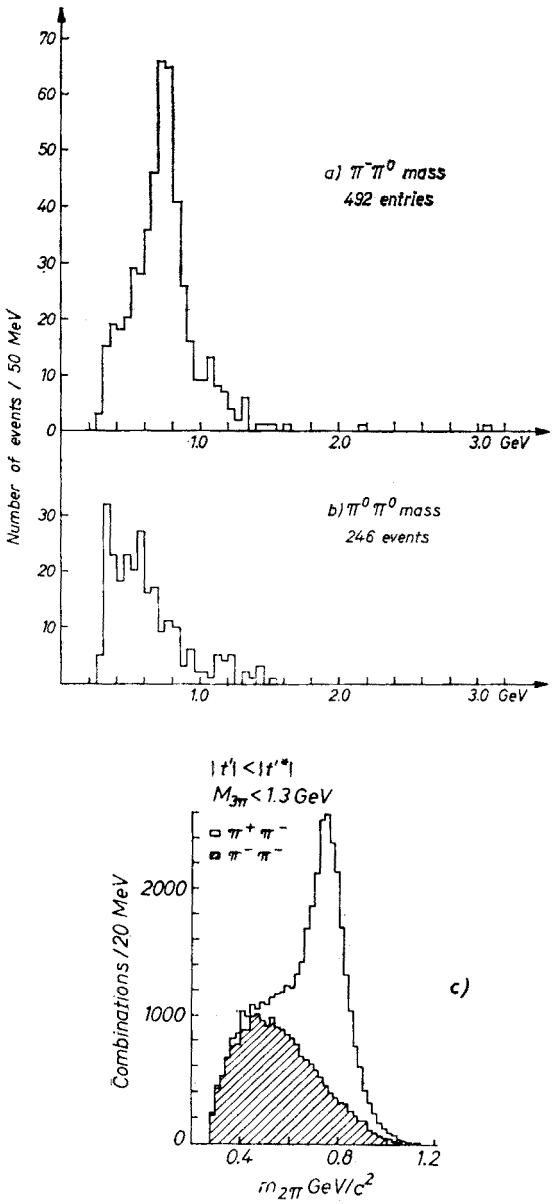

Fig. 8.a), b) $\pi^-\pi^0$ and $\pi^0\pi^0$ effective mass distributions for coherent events (Ref. [9]); c) $\pi^+\pi^-$ and $\pi^-\pi^-$ effective mass distribution for coherent events (Ref. [11])

In addition to the peak at the $\varrho\pi$ threshold there is also a suggestion that there is a peak at the $f^0\pi$ threshold as is seen in the dashed histogram in Figure 7. This enhancement, which peaks near 1.6 GeV, is called the A_3.

A recent bubble chamber experiment on deuterium, by Paler *et al.* [12], where the deuterium is identified by range, momentum, and kinematic fitting in the bubble chamber,

gives similar results. The mass spectra obtained by these experimenters is plotted in Figures 9a, b. This experiment does not have the problem of subtracting an incoherent background since the deuterium can be identified. The use of deuterium gives angle and momentum resolution for the energetic particles which is considerably better than that which

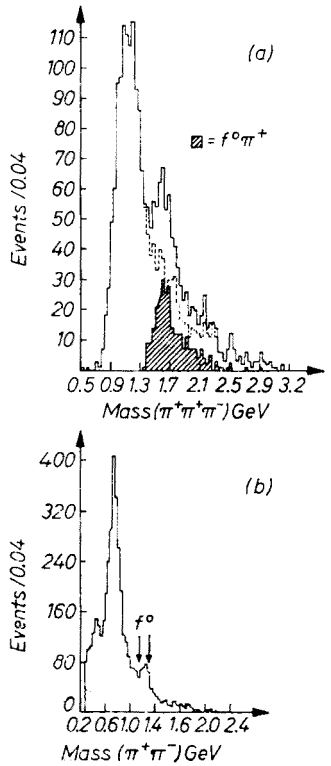

Fig. 9. For the reaction $\pi^+ d \to d\pi^+\pi^+\pi^-$. (a) The $(3\pi)^+$ effective mass distribution. The shaded histogram corresponds to the $f^0\pi^+$ effective mass distribution with f^0 defined as $1.16 < M(\pi^+\pi^-) < 1.32$ GeV. The dashed histogram is the result of subtracting the shaded from the unshaded histogram. (b) The $\pi^+\pi^-$ effective mass distribution for the two combinations from the reaction $\pi^+ d \to d\pi^+\pi^+\pi^-$ (Ref. [12])

can be achieved with the heavy liquids. Notice that in this case there is also a peak at the $f^0\pi$ threshold.

The most interesting point of this experiment is that in addition to the $\varrho\pi$ threshold enhancement there is a very clear $f^0\pi$ threshold effect. A fit to the Dalitz plot by an incoherent sum of ϱ^0 and f^0 symmetrized Breit-Wigner functions and an uncorrelated 3π contribution leads these authors to determine the following limits for the A_3 peak: $> 85\% f^0\pi$, $< 18\%$ $\varrho^0\pi^+$ and $< 5\%$ uncorrelated $\pi^+\pi^+\pi^-$. They find $\varrho\pi$ states which do not contribute to the peak at 1.6 GeV to be present over the entire mass range.

A spin parity analysis of the A_3 mass region leads to the conclusion that $J^P_{A_3}$ is in the series $2^-, 3^+, \ldots$ with 1^+ excluded. A 2^+ assignment cannot be ruled out by the angular distributions.

The high energy optical model developed by Glauber has been applied by Bemporad

et al. to determine the forward A_1N scattering amplitude. The result is that $\sigma_{A_1N} \approx \sigma_{\pi N}$ over the whole mass range [11, 13]. If the $\varrho\pi$ system were a non-interacting system one would expect $\sigma_{A_1N} \geqslant 1.7\,\sigma_{\pi N}$ [14] and the small cross-section was taken on evidence against a non-interacting system. However, Van Hove has pointed out that in diffractive dissociation of hadrons on nuclei the dissociated system can oscillate between many internal states, which makes the nucleus appear more transparent [19]. This effect is discussed in the lectures of Professor Gottfried.

4.2. Nuclear targets ($\pi \to 5\pi$)

Typical t' distributions for the dissociation of a pion into five pions are given in Figures 5a and 10. Also in this case, the t' distributions are determined by the size of the target. Note that the forward coherent peak is not as pronounced as it is in the dissociation

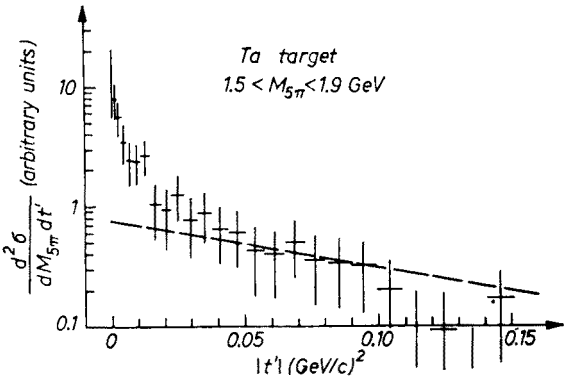

Fig. 10. t' distribution from Ta target for $1.5 < M_{5\pi} < 1.9$ GeV (Ref. [11])

into three pions. This is understood in terms of the five pion mass spectra of Figure 11, obtained by the bubble chamber experiments. The mass spectrum peaks at 1.9 GeV, which, at 15 GeV/c incident momentum, requires a minimum momentum transfer to the target of approximately 130 MeV/c. Hence, the nuclear form factor clearly limits the diffractive dissociation of a pion into five pions.

The five pion mass spectrum obtained by the CERN group and the detection efficiency of their apparatus is shown in Figure 12. Note that the mass spectrum peaks at approximately 1.7 GeV. This shift to lower mass values could be the result of the nuclear form factor, which has a more pronounced effect for the heavier nuclei. In addition, the geometrical efficiency of the apparatus begins to fall off in the region of the peak.

The salient features of the 5π dissociation is that the mass spectrum peaks far from the five pion threshold. It, in fact, peaks near the $\varrho\varrho\pi$ threshold.

At present there does not exist any additional information on this five pion system. Attempts to look for resonant states in the two and three pion submasses have not been conclusive. One must realize that in a $3\pi^- 2\pi^+$ system there are six possible $\pi^+\pi^-$ pairs and $\pi^-\pi^-\pi^+$ triplets and three possible $\pi^+\pi^+\pi^-$ triplets. One is faced with some of the problems encountered in analysing $\bar{p}p$ interactions.

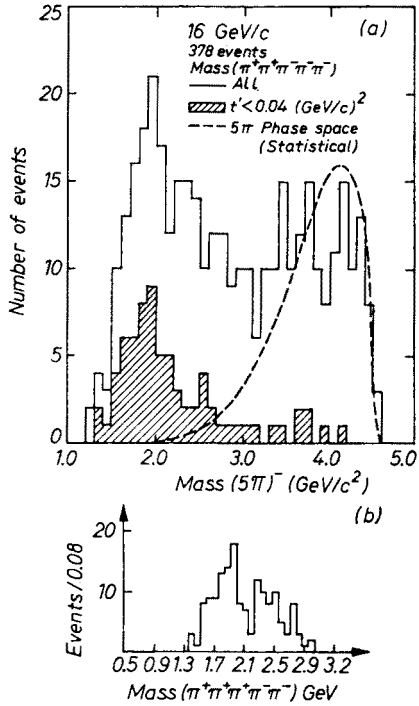

Fig. 11. Five pion effective mass distributions. a) Ref. [15], b) Ref. [12]

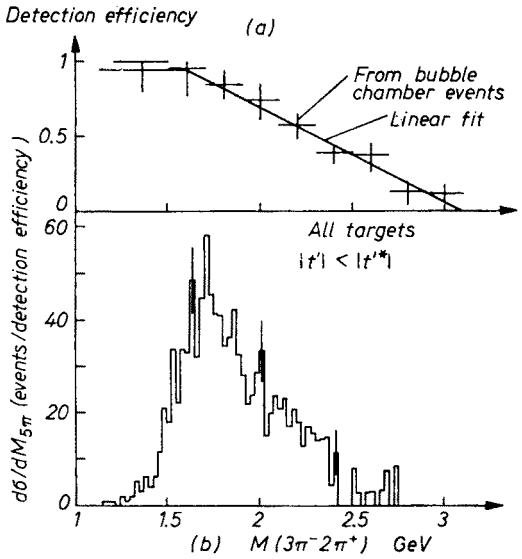

Fig. 12.a) Detection efficiency for $3\pi^- 2\pi^+$ events; b) Effective mass of $3\pi^- 2\pi^+$ events (Ref. [11])

4.3. Nucleon targets

Many experiments have been performed which have studied the reaction $\pi^{\pm}p \rightarrow$ $\rightarrow \pi^{\pm}\pi^{\pm}\pi^{\mp}p$. We shall only discuss briefly some recent experiments at incident momenta greater than 10 GeV/c.

In Figure 13a, b the combined $\pi^+\pi^-\pi^-$ mass spectrum obtained by the Harvard group [16] from experiments at 13 and 20 GeV/c is shown. The interesting point is that

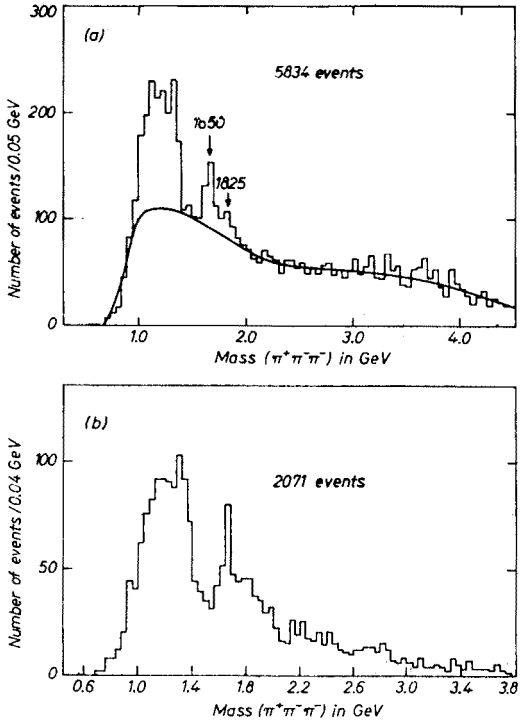

Fig. 13. The $\pi^+\pi^-\pi^-$ effective mass distribution from the reaction $\pi^-p \rightarrow 2\pi^-\pi^+p$ at 13 and 20 GeV/c (Ref. [16]). a) all events; b) $1.15 < m(p\pi^+) < 1.35$ GeV and $0.05 < |t_{pp}| < 0.25$ (GeV/c)^2

these data also show a threshold effect at 1.1 GeV (A_1) as well as an $f^0\pi$ threshold effect at $\sim$1.65 GeV (A_3). The low mass region is broader than that observed in the nuclear target experiments. This is due to A_2 production, which because it is a 2^+ state is suppressed at small t on nuclear targets. A Dalitz plot analysis leads these authors to conclude that there is a 3π as well as an $f^0\pi$ contribution to the A_3. There is also $\varrho\pi$ in the A_3 region which is the tail of the A_1 and A_2. They claim some evidence for an additional enhancement at $\sim$1.8 GeV, which requires confirmation by other experiments.

An experiment of the Durham–Genova–Hamburg–Milano–Saclay Collaboration at 11.7 GeV/c [17] has given similar results as one can see from the mass spectrum shown in Figure 14. Again, the threshold effect of the A_1 is combined with the A_2, and a clear A_3 is observed. A very detailed spin parity analysis by this group using a three-particle partial wave analysis leads to the conclusion that the $f^0\pi$ threshold enhancement is an s-wave $J^P =$ $= 2^-$. They also find that the $\varrho\pi$ states have predominantly $J^P = 1^+$ ($L = 0$) over the whole

mass range. There is no significant $\varepsilon\pi$ in the 2^- partial wave. They do, however, observe structure in the $J^P = 0^- \varepsilon\pi$ state. These authors point out that the $J^P = 0^- \varepsilon\pi$ matrix element resembles a phase space distribution on the Dalitz plot. The chief result of this

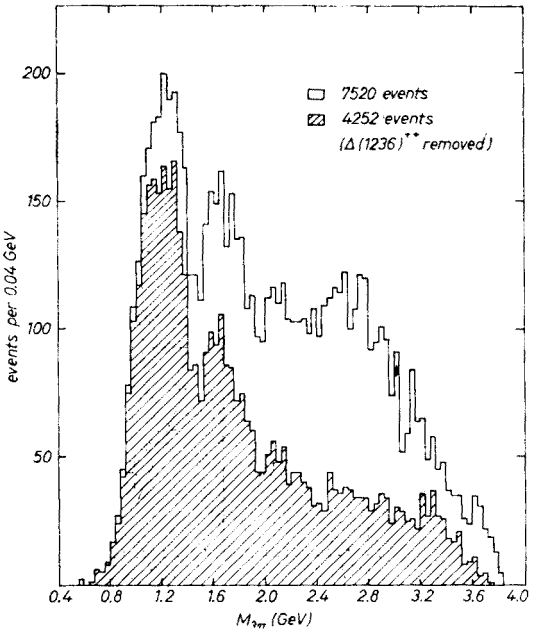

Fig. 14. The $2\pi^+\pi^-$ effective mass distribution from the reaction $\pi^+p \to 2\pi^+\pi^-p$ at 11.7 GeV/c (Ref. [17])

work is that the A_3 enhancement is mainly an $L = 0$ $f^0\pi$ threshold effect, similar in nature to the A_1 which has been found in most experiments to be mainly a $\varrho\pi$ ($L = 0$) threshold effect.

A recent SLAC experiment by Ballam *et al.* [18] has studied the reactions $\pi^\pm p \to$ $\to \pi^\pm\pi^\pm\pi^\mp p$ at 16 GeV/c. The longitudinal phase space plot [7] is used for separating the events into subsets corresponding to various reaction mechanisms. Events which are candidates for diffractive dissociation of the pion have all three pions moving forward in the CMS. The momentum transfer to the target proton for these events is given in Figure 15, and there seems to be an excess of events in the region $t' < 0.08$ (GeV/c)^2. It is interesting to note that the three pion effective mass spectrum (Figure 16) for $t' < 0.08$ is almost identical to that obtained in diffractive dissociation experiments from nuclei, *i.e.* an amorphous blob, whereas the region $t' > 0.08$ seems to show some structure (note, this is not a high statistics experiment). Neglecting the ten-event spike at 1.08 GeV, there is nevertheless a spike at 1.3 GeV which was not present in the events for $t' < 0.08$. The decay angular distributions also differ in the two t' regions.

It is interesting to note that the use of nuclear targets automatically restricts one to the region $t' < 0.1$ (GeV/c)^2, and the similarity between nuclear production and single nucleon production at small t may be more than fortuitous. In order to illustrate this point the compilation of the three pion mass spectra obtained from coherent production

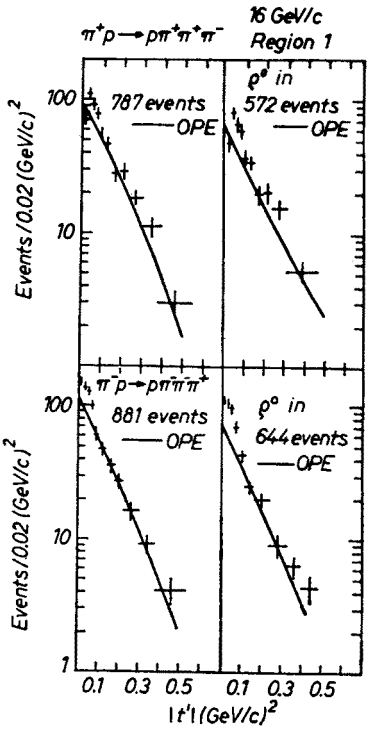

Fig. 15. t' distributions for events in the diffractive dissociation region of the Van Hove plot (Ref. [18])

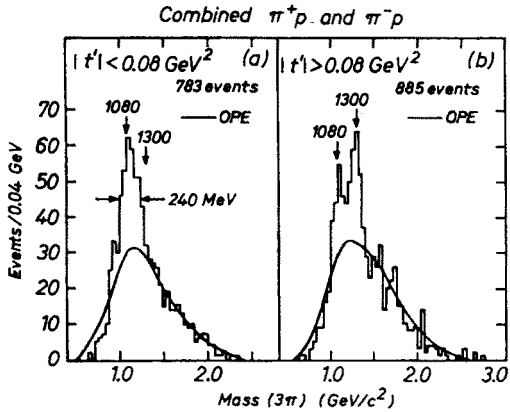

Fig. 16. Three pion effective mass distributions (Ref. [18]). a) $t' < 0.08$ (GeV/c)^2; b) $t' > 0.08$ (GeV/c)^2

on Be, Cu, Al, Si, Ti, Ag, Ta and Pb by the CERN experiment has been plotted with the SLAC $t' < 0.08$ (GeV/c)^2 mass spectrum in Figure 17[2]. Clearly, the mass spectra are compatible.

[2] This required binning the high statistics data of Bemporad *et al.* [11] in 40 MeV bins, which was done from the published curves. The author appologizes to the experimenters for any errors which he may have introduced.

The Illinois group [20] has compiled most of the available $\pi^- p$ data in which A_1^- production is observed. This data covers the range from 5 to 25 GeV/c in pion momenta. The $J^P = 1^+$ contribution in the A_1 region (1.0−1.2 GeV) was extracted by a partial

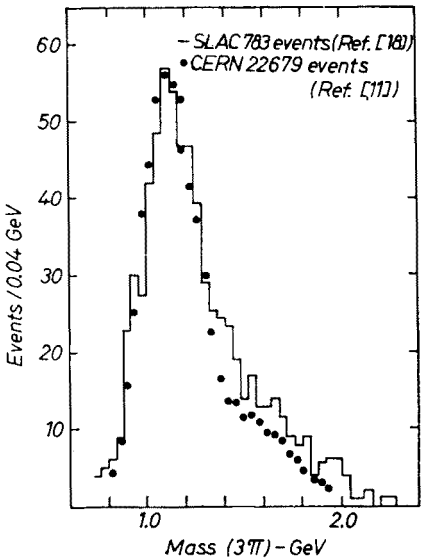

Fig. 17. Comparison of three pion effective mass spectra. — Hydrogen results of Ref. [16] at 16 GeV/c. ● Compilation of coherent production on Be, C, Al, Si, Ti, Ag, Ta, Pb of Ref. [11] at 15.1 GeV/c (coherent production data scaled to hydrogen data at peak of distribution)

wave analysis. The production cross-section for the 1^+ $\varrho\pi$ state decreases with incident momentum as $P_{\mathrm{LAB}}^{-0.5}$. The ϱ_{00} density matrix element was determined in both the s- and t-channel helicity frames; the results, which are summarized in Table I, favor t-channel helicity conservation. Similar conclusions were reached by the ABBCCHLV collaboration [21], who have also reported a cross over effect in A_1 production [22].

TABLE I

A_1^- density matrix elements (Ref. [20])

		t-channel helicity frame $\Delta^2-\Delta^2_{\min}$			s-channel helicity frame $\Delta^2-\Delta^2_{\min}$		
		0.0−0.1 (GeV/c)^2	0.1−0.2 (GeV/c)^2	0.2−0.4 (GeV/c)^2	0.0−0.1 (GeV/c)^2	0.1−0.2 (GeV/c)^2	0.2−0.4 (GeV/c)^2
ϱ_{00}	Low-energy[a]	0.94±0.02	0.93±0.05	0.87±0.07	0.89±0.02	0.74±0.03	0.41±0.06
ϱ_{00}	High-energy[b]	0.96±0.05	0.95±0.12	0.98±0.20	0.94±0.05	0.77±0.08	0.46±0.13
$\mathrm{Re}\varrho_{10}$	Low-energy	−0.08±0.01	−0.13±0.02	−0.09±0.03	0.16±0.01	0.28±0.02	0.31±0.04
$\mathrm{Re}\varrho_{10}$	High-energy	−0.10±0.02	−0.13±0.04	−0.06±0.07	0.15±0.02	0.28±0.05	0.35±0.08

[a] Low energy is the sum of the 5-. 7-, and 7.5-GeV/c data.
[b] High energy is the sum of the 11-, 13-, 20-, and 25-GeV/c data.

4.4. Summary

Pions have been observed to dissociate into both three and five pions. In each case the target seems to play no role. The three pion effective mass distributions strongly suggest the dominance of $\varrho\pi$ and $f^0\pi$ threshold effects. The $\varrho\pi$ system seems to be dominated by the $J^P = 1^+ (L = 0)$ partial wave. Some 10 to 20% D-wave is not excluded. The data favor a $J^P = 2^- (L = 0)$ state for the $f^0\pi$ system. It is still not clear whether the A_1 and A_3 regions contain resonances. For the A_1 this confusion has existed for almost 10 years!

The data favor t-channel helicity conservation for the A_1. The similarity between the mass spectra obtained from coherent nuclear interactions and single nucleon production at small t suggests that nuclear targets are particularly useful for studying diffractive dissociation at small t.

The production mechanism for the A_1 is probably not entirely diffractive dissociation, since the $J^P = 1^+$ cross-section seems to be falling with energy and a cross over effect is observed.

5. *K-dissociation*

The K has been observed to dissociate into a $K\pi\pi$ system which is similar to the three pion system obtained in pion dissociation, and there is an indication of dissociation into the $K\pi\pi\pi$ system.

5.1. Experimental difficulties

Experiments performed to date on the $K^-\pi^+\pi^-$ final states have not been able to unambiguously identify the K^-. The experimenters have relied on various Monte Carlo studies in order to determine the best way to choose which of the two negative particles is the K^-. The details of how the K^- selection is made and how the biases introduced by the selection criteria are removed from the data is beyond the scope of this paper. It is a very difficult problem, and each experimental group has a slightly different procedure. It is likely that the different procedures could account for some of the differences in the $K^*\pi$ and $K\varrho$ distributions which have been published.

5.2. Further complications

From general quark model considerations a $J^P = 1^+$ state can be formed from a $^3P_1$ or $^1P_1$ $q\bar{q}$ state. The former has $C = +1$ (A_1 nonet) while the latter has $C = -1$ (B nonet). The $K\pi\pi$ system can have contributions from both $J^P = 1^+$ and $J^P = 1^-$ (G-parity spares the 3π system from this additional complication). The result is that one must consider the possibility of two states K_A and K_B which can mix to give physical states Q_A and Q_B, and the physical states may interfere [23]. If there is no interference, then only Q_A will be produced in reactions in which $C = +1$ exchanges are the only ones possible. In this case nuclear targets which enhance isoscalar, non-spin-flip couplings are probably not sufficient, since ω exchange is allowed.

5.3. Nuclear targets

Experimental results are available from heavy liquid bubble chambers using K^- beams at 5, 10 and 12.7 GeV/c. The BNL–U. C. Berk.–Milan–Saclay–Orsay collaboration [24] has studied the reactions

$$K^-\mathcal{N} \to K^-\pi^+\pi^-\mathcal{N} \tag{5.1}$$

$$K^-\mathcal{N} \to K^0\pi^-\pi^0\mathcal{N} \tag{5.2}$$

$$K^-\mathcal{N} \to K^-\pi^0\pi^0\mathcal{N} \tag{5.3}$$

Because these experiments are performed in heavy liquids the γ rays from the π^0 decays are observed and measured. In addition all events in reaction (5.2) have an observed K^0 decay which is measured.

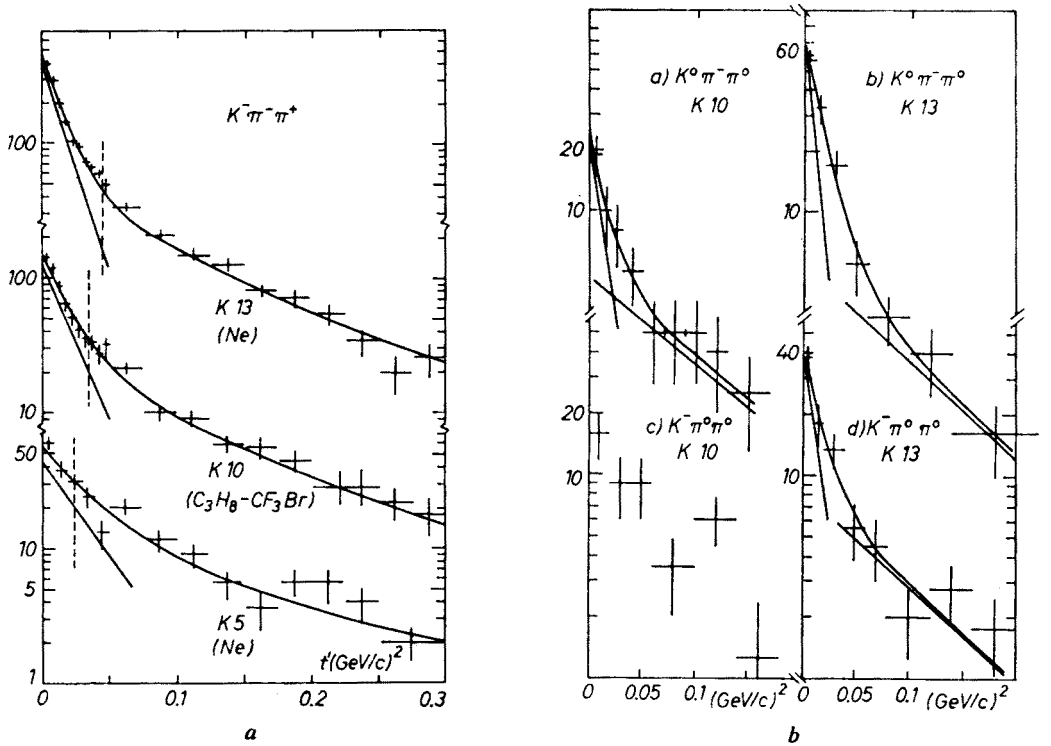

Fig. 18. t' distribution for $K2\pi$ production. Curves are the result of fitting to two exponentials (Ref. [24])

In Figure 18 the t' distributions obtained for the above reactions are shown. In each case one observes the sharp forward peak in t' which is compatible with a coherent interaction with the nucleus in question. In Figure 19 the t' distributions for production from neon, deuterium and hydrogen are compared, and the effect of the target size is clear.

The $K\pi\pi$ mass distribution found by these experimenters is given in Figure 20, where they compare with results on hydrogen and deuterium. They find an enhancement in the

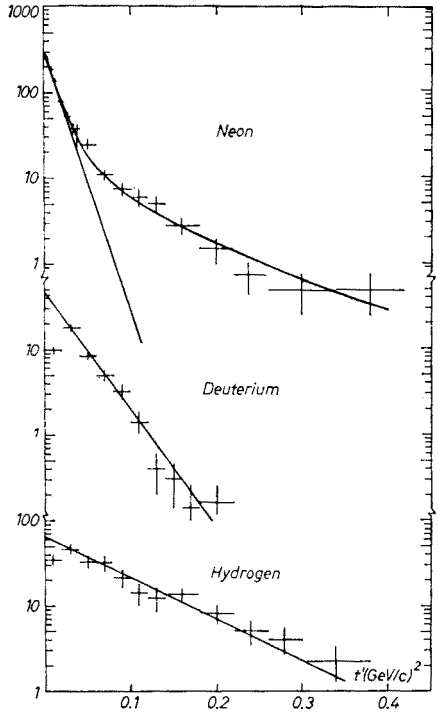

Fig. 19. t' distribution for Q production on hydrogen, deuterium and helium (data from Fournier's thesis) Ref. [24])

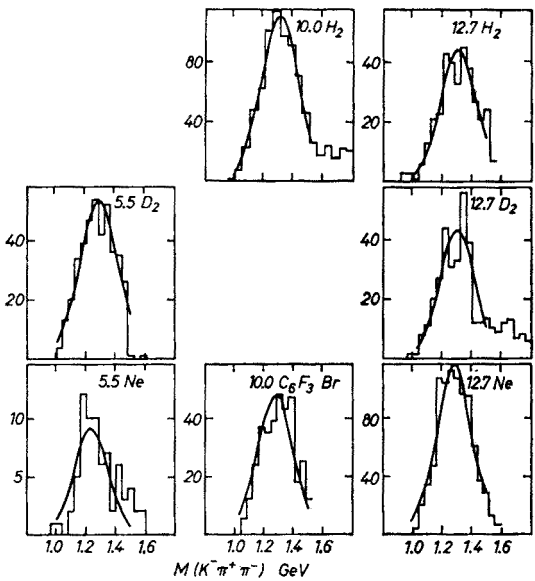

Fig. 20. $K^-\pi^+\pi^-$ effective mass spectra from interactions at 5.5, 10 and 13 GeV/c on nuclei ($A \approx 20$), deuterium, and hydrogen for small t' and $0.8 < m_{K^-\pi^+} < 1.0$ GeV. The curves are Gaussian forms with mean value 1.3 GeV, which have been scaled by the nuclear form factor where appropriate. (From Fournier's thesis, Ref. [24])

region of 1.0 to 1.5 GeV, which is usually called the Q region. These mass spectra are better represented by a Gaussian distribution than by a Breit-Wigner distribution. The mean value of the distribution is at approximately 1.3 GeV. The L enhancement which is observed in experiments on hydrogen targets is suppressed by the nuclear form factor at these energies. The effect of the nuclear form factor in the L region is shown in Figure 21.

In reactions (5.1) and (5.2) both $K^*\pi$ and $K\varrho$ final states are possible and both are observed. The various fractions are given in Table II. tan α gives the ratio of decay ampli-

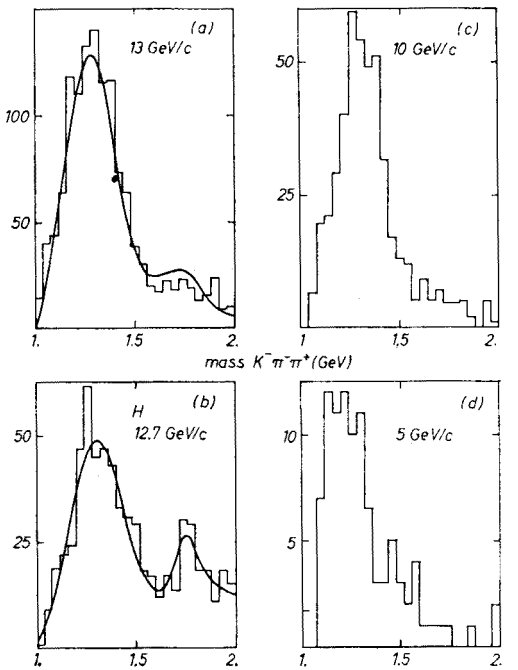

Fig. 21. $K^-\pi^+\pi^-$ effective mass spectra. a, c, d) spectra obtained in K^-Ne interactions; b) spectrum obtained from K^-p interactions. The curve in a) is the result of multiplying the curve in b) by the nuclear form factor (from Fournier's thesis, Ref. [24])

TABLE II

Decay parameters of the Q. tan α is the ratio of decay amplitudes into $K\varrho$ and $K^*\pi$ and φ the relative phase (Ref. [24])

Channel	α(rad)	φ(rad)	Percent Background	Percent K^*	Percent ϱ	Percent Intg $K\varrho$
$K^-\pi^0\pi^0$ 10+12.7 GeV/c	0 (fixed)	—	$(48\pm12)\%$	$(52\pm12)\%$	—	—
$K^0\pi^-\pi^0$ 10+12.7 GeV/c	0.39 ± 0.06	3.50 ± 0.40	$(1\pm{}^{10}_{1})\%$	$(70\pm5)\%$	$(16\pm4)\%$	$(13\pm3)\%$
$K^-\pi^+\pi^-$ 12.7	0.63 ± 0.05	3.00 ± 0.20	$(8\pm5)\%$	$(61\pm4)\%$	$(21\pm4)\%$	$(10\pm4)\%$
$K^-\pi^+\pi^-$ 10.0	0.61 ± 0.08	2.50 ± 0.30	$(9\pm7)\%$	$(62\pm5)\%$	$(19\pm4)\%$	$(10\pm4)\%$
$K^-\pi^+\pi^-$ 5.5	0.29 ± 0.15	3.05 ± 0.80	$(14\pm10)\%$	$(76\pm10)\%$	$(5\pm{}^{5}_{3})\%$	$(5\pm8)\%$

tudes into $K\varrho$ and $K^*\pi$ in the Q region. There is roughly a five standard deviation difference in α between channel (5.2) and channel (5.1). A study of the decay angles of the K^*_{890} gives $J^P = 1^+ (L = 0)$ for the Q region.

The $K\pi^0\pi^0$ shows a much larger background than the other two channels, which the experimenters claim may be the result of spurious γ's which are incorrectly assigned to a π^0 vertex.

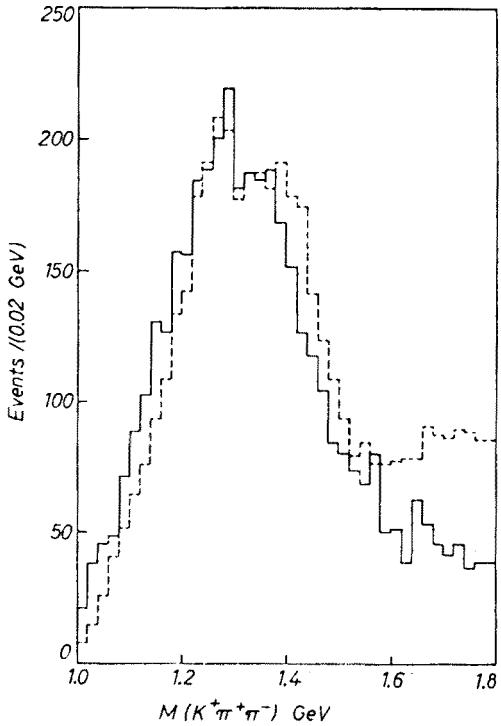

Fig. 22. $K^+\pi^+\pi^-$ effective mass spectrum. $K^+d \to K^+\pi^+\pi^-d$ (Ref. [25]); $K^+p \to K^+\pi^+\pi^-p$ (Ref. [26])

By using the results of Q production on nuclei and applying the Glauber model these experimenters have found $\sigma_{QN}/\sigma_{KN} \simeq 1$.

Experiments on deuterium have given results which are similar to the above. The reaction

$$K^+d \to K^+\pi^+\pi^-d \tag{5.4}$$

has been studied by Firestone *et al.*, [25] and they obtain the mass spectrum shown in Figure 22; the dashed curve is a compilation of K^+p data in the momentum range 7.3 to 12.7 GeV/c; the two distributions are remarkably similar. The suppression of K^*_{1420} production (a 2^+ state) on deuterium accounts for the differences near 1.4 GeV. A good fit to the deuterium mass spectrum is obtained with two Breit-Wigner forms. The parameters are $M_A = 1.23$ GeV and $M_B = 1.37$ GeV with width $\Gamma_A \simeq 190$ MeV and

$\Gamma_B \simeq 240$ MeV. Similar parameters have been obtained for the hydrogen data [26]. A study of the decay angular distributions gives $J^P = 1^+ (L = 0)$ with mainly $K^*_{890}\,\pi$ decay for the Q region.

5.4. Nucleon targets

Reactions (5.1) and (5.2) have also been studied in hydrogen bubble chambers. The presence of a K is infered from a kinematic fit. These experiments give results which are similar to those discussed above. Namely, the $K\pi\pi$ mass spectrum is found to be dominated

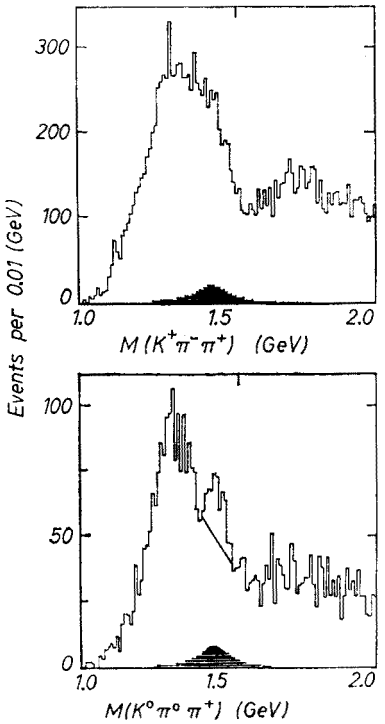

Fig. 23. The $K\pi\pi$ effective mass spectra with no cuts. Shaded events are estimates of $K^*(1420)$

by a peak at 1.3 GeV (the Q) with a second peak at ~ 1.8 GeV (the L). The experiments give results which favor the assignments $J^P_Q = 1^+$ and $J^P_L = 2^-$ with the Q decaying into s-wave $K^*_{890}\pi$ and $K\varrho$ while the L contains significant s-wave $K^*_{1420}\pi$.

The reactions $K^+p \to K^+\pi^+\pi^-p$ and $K^+p \to K^0\pi^0\pi^+p$ have been studied at 12 GeV/c by group A at LBL [27]. The $K\pi\pi$ mass spectra show the characteristic Q and an indication of an L. There are differences in the spectra obtained for the two charge states (Fig. 23). The $K^0\pi^0\pi^+$ events have two peaks, one at 1.26 GeV with $\Gamma \simeq 120$ MeV and one at 1.42 GeV with $\Gamma \simeq 80$ MeV of which over half can be attributed to the $K^*(1420)$. The $K^+\pi^+\pi^-$ mass spectrum has a different shape (no dip at 1.36 GeV). The authors suggest that this difference may be due to the presence of a $T = 0$, s-wave $\pi\pi$ state in the $K\pi\pi$ system. The 1.26 GeV region is produced more peripherally than the 1.42 GeV region (see Table III).

The observed Q is mainly $K^*(890)\pi$ with some ϱK. The presence of several J^P states is found, but the 1^+ ($L = 0$) dominant. This high statistics experiment (35 events/μb) illustrates the complexity of the $K\pi\pi$ system.

An interesting result has been obtained by a SLAC group in the study of the reaction

$$K_L^0 p \to K_S^0 \pi^+ \pi^- p$$

in the SLAC 40 inch hydrogen bubble chamber [28]. The momenta of the K_L^0 covered the range from 4 to 12 GeV/c. In this final state both Q and $\overline{Q}$ production can be studied by selecting $0.86 < M(K_S^0\pi^+) < 0.92$ GeV and $0.86 < M(K_S^0\pi^-) < 0.92$ GeV, respectively. The authors exclude events in the $K^*(890)$ overlap and require $M(p\pi^+) > 1.34$ GeV. The differential cross-sections for Q and $\overline{Q}$ production given in Figure 24 show the characteristic cross over effect observed in Kp elastic scattering. The experimentally determined cross

TABLE III

Fits of $e^{Bt_{pp}}$ to t_{pp} spectra of $K\pi\pi$ (Ref. [27])

$M(K\pi\pi)$ region (GeV)	B in GeV^{-2} (confidence level)	
	$pK^+\pi^-\pi^{+a}$	$pK^0\pi^0\pi^{+b}$
(I) 1.1 to 1.2	$9.5\pm0.4(5.2\times10^{-1})$	$8.3\pm0.6(8.1\times10^{-1})$
(II) 1.2 to 1.27	$9.0\pm0.3(3.6\times10^{-3})$	$7.9\pm0.5(1.6\times10^{-2})$
(III) 1.27 to 1.36	$7.6\pm0.3(9.7\times10^{-2})$	$6.9\pm0.5(2.6\times10^{-1})$
(IV) 1.36 to 1.46	$6.5\pm0.2(1.2\times10^{-4})$	$6.1\pm0.5(5.7\times10^{-1})$
entire Q	$7.9\pm0.1(1.8\times10^{-9})$	$6.9\pm0.5(7.7\times10^{-2})$[a]

[a] Fits are to t_{pp} from 0.0 to 0.4 GeV^2 in 0.05-GeV^2 bins.
[b] Fits are to t_{pp} from 0.0 to 0.4 GeV^2 in 0.1-GeV^2 bins.

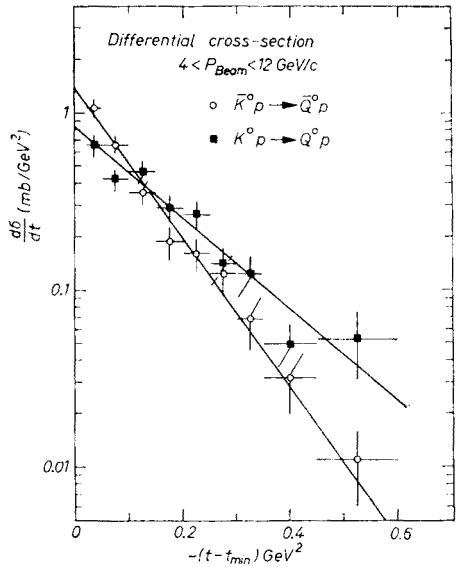

Fig. 24. Differential cross-section for Q^0 and $\overline{Q}^0$ production (Ref. [28])

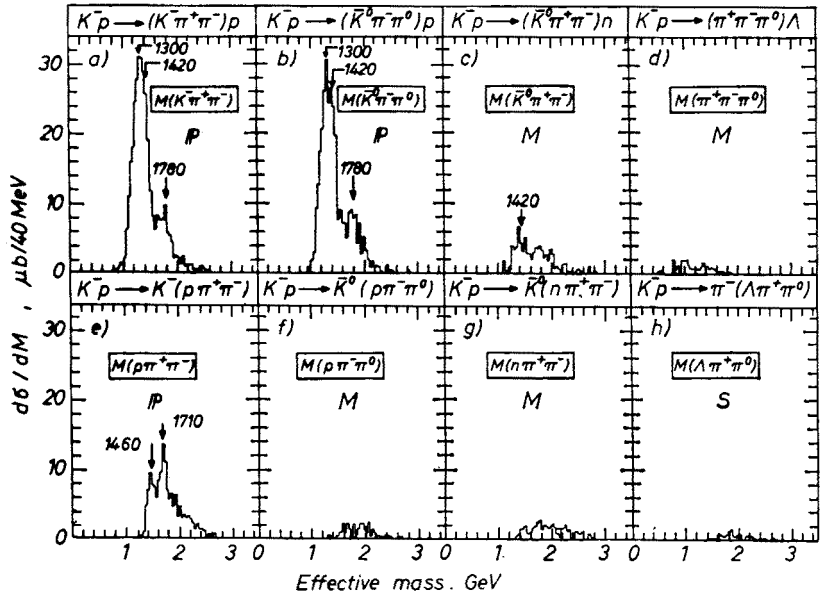

Fig. 25. Effective mass distribution for events in which three particles move forward (a–d) and backward (e–h) in the CMS (Ref. [29])

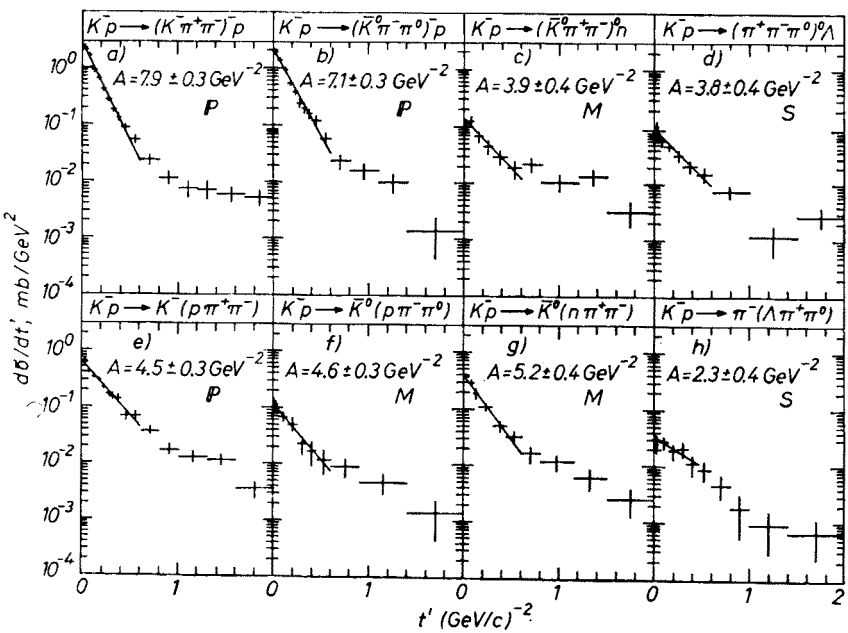

Fig. 26. t' distributions for events in which three particles move forward (a–d) and backward (e–h) in the CMS. Curves are fits to the form $e^{-At'}$ in the interval $0 < t' < 0.6$ (GeV/c)^2 (Ref. [29])

over point is at $t' = 0.13 \pm 0.03$ (GeV/c)^2 and the slopes of the forward peaks are $B_Q = 5.9 \pm 0.5$ (GeV/c)$^{-2}$ and $B_{\bar{Q}} = 9.7 \pm 0.7$ (GeV/c)$^{-2}$. The authors point out that in the momentum interval 5 – 10 GeV/c the elastic K^+p and K^-p differential cross-sections have slopes $B = 5.5$ and 7.5 (GeV/c)^2 respectively.

Diffractive dissociation in K^-p interactions has been studied by the Aachen–Berlin–CERN–London–Vienna collaboration using longitudinal phase space techniques to separate various production mechanisms [29]. The effective mass distributions for the three particle states which go forward in the CMS and their corresponding $d\sigma/dt'$ distributions are given in Figures 25, 26. Clearly, the reactions for which vacuum quantum number exchange is possible (Figures 25a, b) dominate the four body final states. Both the Q and L enhancement are visible. The $\bar{K}^0\pi^+\pi^-$ states (Figure 25c) which involve charge exchange are dominated by $K^*(1420)$ production — no Q or L signal is observed.

The $d\sigma/dt'$ distributions fitted to $\exp(At')$ give forward slopes which are compatible with values obtained in K^-p elastic scattering. It is amusing to note that for $t \gtrsim 0.6$ GeV^2 there is a break in the t' distribution. A similar result has been observed in Figure 18 for production from nuclei, where the change in slope results from the substructure of the nucleus, *i.e.*, interactions in which nucleons are excited into the continuum.

There is general agreement that s-channel helicity is not conserved in Q production; however, it is not clear that t-channel helicity is conserved [30].

5.5. Summary

The dissociation reaction $K \to K\pi\pi$ has been studied for both charged and neutral final states. The $K\pi\pi$ effective mass spectra are dominated by a $K^*(890)\pi$ and ϱK threshold effect (the Q-enhancement) and a $K^*(1420)\pi$ threshold effect (the L-enhancement). This latter effect is not as well studied as the corresponding A_3 in pion dissociation. The Q-region is mainly s-wave $K^*(890)\pi$ which gives $J_Q^P = 1^+$. There are indications that the L results in part from s-wave $K^*(1420)\pi$ which gives $J_L^P = 2^-$.

The Q region is complicated, since there may be two objects with different C-parity, contributions from the $K\pi\pi$ decay of the $K^*(1420)$, and ϱK and εK contributions. The experimental difficulty in unambiguously identifying the K limits the ability of present experiments to resolve some of the above problems.

The observation of a very strong cross over effect indicates that the Q production mechanism has a large non-diffractive contribution.

The mass spectra obtained from dissociation on nuclear targets agrees well with the hydrogen results if the nuclear form factor is taken into account.

All experiments agree that Q production does not conserve s-channel helicity; the evidence for t-channel helicity conservation is not conclusive. It may be that Q production conserves neither s-nor t-channel helicity.

6. Nucleon dissociation

The dissociation of nucleons into two and three bodies has been observed. In this case the nucleon which dissociates can be either at rest (the target) or moving in the laboratory (the incident particle).

6.1. Nuclear targets

A recent experiment at the Brookhaven AGS has studied the reaction

$$n + \mathcal{N} \rightarrow \pi^- p + \mathcal{N}$$

using several nuclei as targets [31]. The momentum of the neutron beam covered the range 10 to 30 GeV/c. The experimental arrangement is shown in Figure 27. The resolution of the spectrometer gave ± 1.2 mr. in the pair opening angle and $\Delta p/p \approx 1.5\%$ at 15 GeV/c. Since the momentum transfer in such processes is small, the momentum of the incident

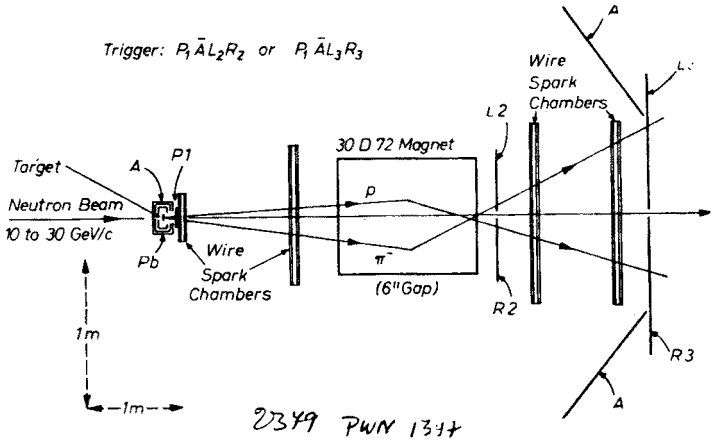

Fig. 27. Experimental arrangement of Longo *et al.* (Ref. [31])

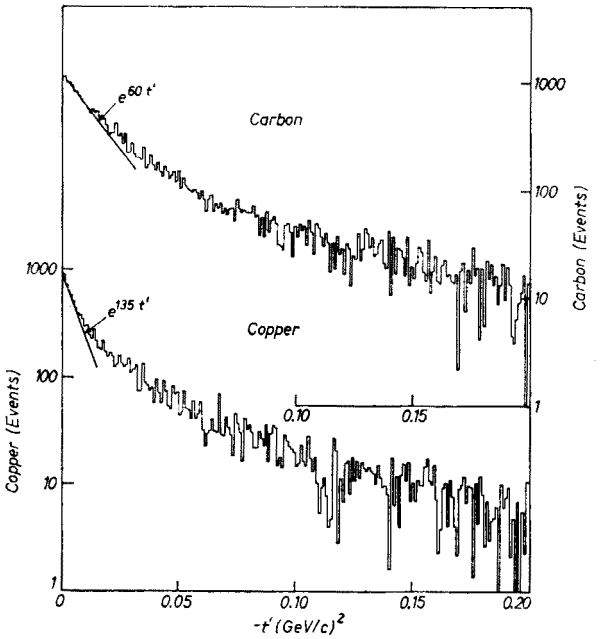

Fig. 28. t' distribution for the reaction $n + \mathcal{N} \rightarrow p\pi^- + \mathcal{N}$ from C and Cu targets. The straight line is a hand fitted slope (Ref. [31])

neutron can be calculated from the measured momentum of the π^- and p. As a result, the diffractive dissociation process $n \to \pi^- p$ can be used as a technique for determining the momentum spectrum of a neutron beam.

The momentum transfer distributions are given in Figure 28; the sharp forward peak which is compatible with the nuclear radius verifies that a coherent process is observed.

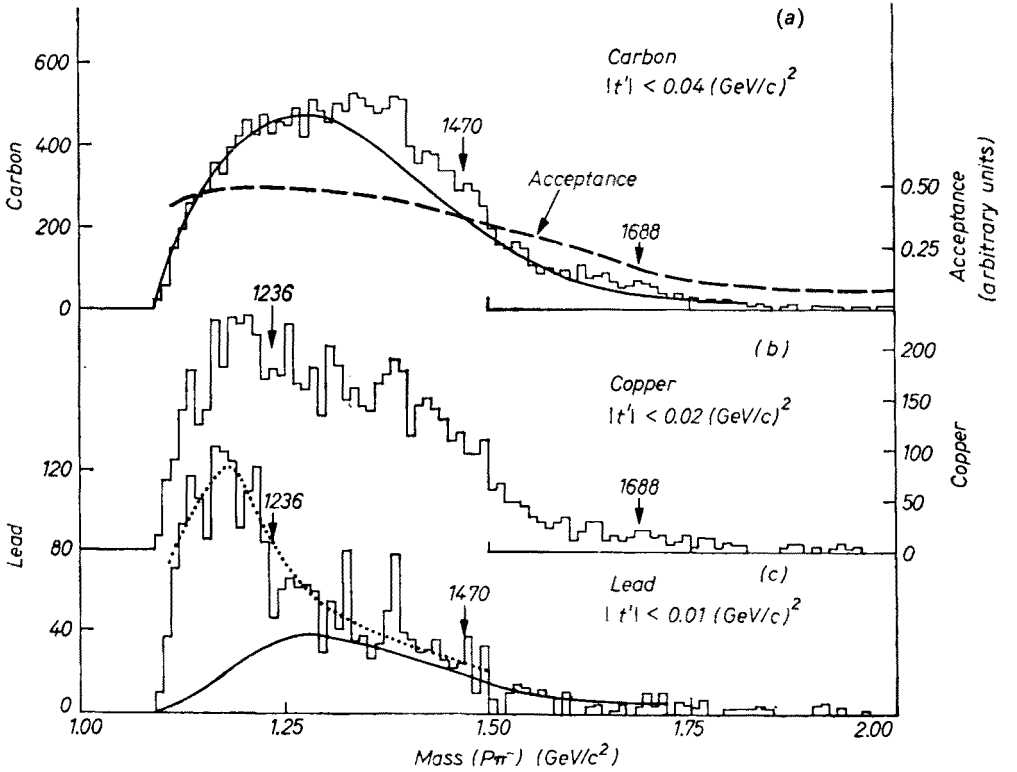

Fig. 29. Effective mass of $p\pi^-$ system. The dashed line in (a) gives the experimental efficiency which has not been unfolded (Ref. [31])

The $p\pi^-$ effective mass distributions, Figure 29, show no indication of any resonance structure. One might expect that the well-known $T = 1/2$ baryon resonances near 1.5 and 1.7 GeV would be present. The minimum momentum transfer "cut-off" does not explain the absence of resonance structure.

Typical angular distributions obtained by these authors are given in Figure 30. Because the geometrical acceptance data exist only for $\cos\theta_\pi > -0.04$; the angular distributions have been corrected for detection efficiency. The experimenters conclude that coherent production gives $p\pi^-$ states with $J \geqslant 3/2$; however, they cannot exclude the possibility of a mixed state which is 80% $J^P = 1/2^+$ and 20% $J^P = 3/2^+$.

Nucleon dissociation into three bodies has not been studied extensively on nuclear targets. There is an old, low-statistics experiment studying the reaction $p + \mathrm{Ne} \to p\pi^+\pi^- + \mathrm{Ne}$ [33] which gives an enhancement in the $p\pi^+\pi^-$ mass spectrum near 1.4 GeV and an indica-

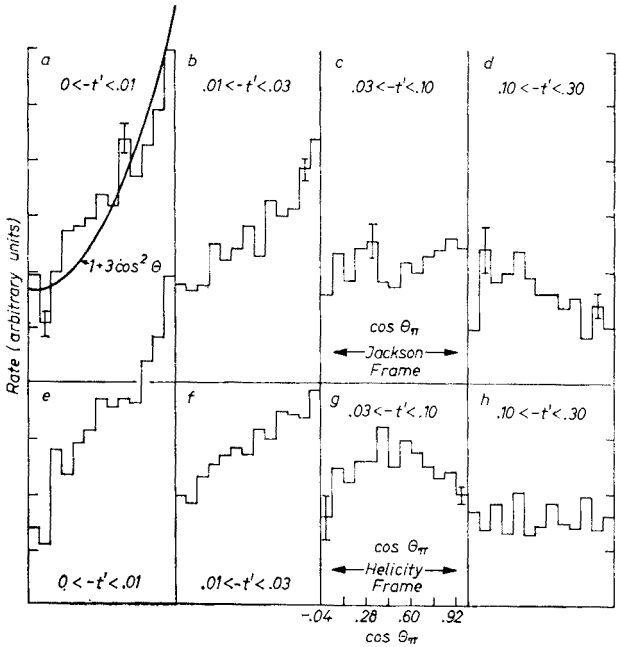

Fig. 30. Distributions in the cosine of the polar angle of the π in the $p\pi^-$ rest frame with $1.1 < m(p\pi) < 1.32$ GeV; the higher mass region gives similar results. Carbon data only. (Ref. [32])

tion that the cross-section of the $p\pi^+\pi^-$ system on nucleons is compatible with 40 mb (*i.e.*, the nucleon-nucleon cross-section).

6.2. Nucleon targets

The reactions

$$p+p \to p+\text{missing mass} \tag{6.1}$$

$$\pi+p \to \pi+\text{missing mass} \tag{6.2}$$

have been studied by a BNL Carnegie-Mellon collaboration [34, 35]. In (6.1) a recoil spectrometer was used. Data were taken at incident proton momenta of 6.2, 9.9, 15.1, 20.0 and 29.7 GeV/c and over a t-range of $0.01-0.5$ (GeV/c)^2. In (6.2) a single arm spectrometer was used to measure the momentum and angle of the pion. Data were taken at 8 and 16 GeV/c incident momenta and over a t range of $0.05-1.5$ (GeV/c)^2. Typical missing mass distributions obtained in these experiments is given in Figure 31. The well known $\Delta(1236)$ and the $T = 1/2$ isobars at 1410, 1500, 1690 and 2190 MeV are observed. Typical t distributions are given in Figure 32. It should be noted that there is some evidence in both reactions for shrinking of the forward diffraction peak, which would be consistent with the usual Regge model interpretation. Also, in reaction (6.2) there is a suggestion that $d\sigma/dt$ may be going to zero in the forward direction for all isobars except the $N^*(1400)$.

In the region where it is applicable the $d\sigma/dt$ distributions have been fit to e^{bt}. The results at 15 GeV/c are summarized in Table IV, where the results of a fit of the integrated cross-section to a form p_{LAB}^{-n} is also presented.

A preliminary publication of the results from reaction (6.1) indicated that the integrated cross-sections of the $T = 1/2$ isobars were nearly energy independent [36]; however,

the final paper gives the results quoted in Table IV. The normalization in such missing mass experiments is always difficult. In this instance the measured elastic cross-section does not extrapolate well to the optical point and must be scaled. The shape of the elastic

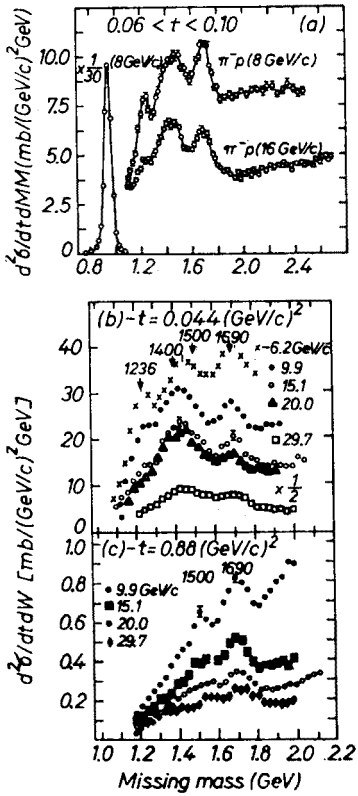

Fig. 31

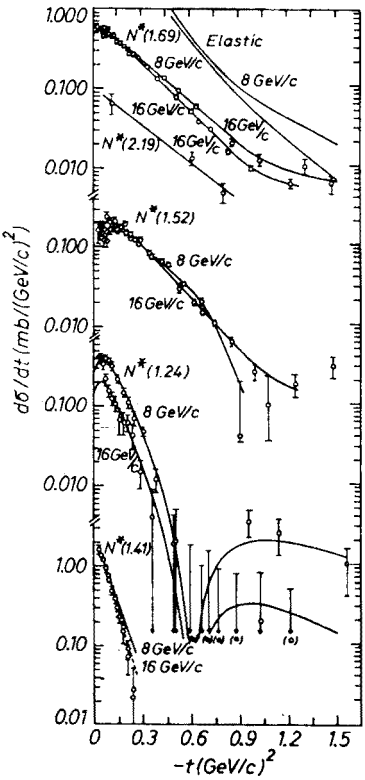

Fig. 32

Fig. 31. Typical missing mass spectra for the reactions. a) $\pi^- p \to \pi^- + MM$ (Ref. [34]); b, c) $pp \to p + MM$ (Ref. [35])

Fig. 32. $d\sigma/dt$ for various N^*'s in the reaction $\pi^- p \to \pi^- N^*$ at 8 (○) and 16 (□) GeV/c. Curves of the $\Delta(1236)$ are from the pp data of Ref. [35]. In all other cases the straight line portion at small t is obtained by a fit to exp (bt) (see Table IV), while the rest of the curve is sketched

TABLE IV

Values of b and n from fits to $d\sigma/dt \sim \exp(bt)$ and $\sigma_{N^*} \sim p_{LAB}^{-n}$

	1236	1410	1500	1690	2190	Elastic
b_{pp}	[a]10±1	16±3	4.7±3	4.7±0.2	5±0.6	9±0.2
$b_{\pi p}$	10±2	16±1.3	5.1±0.15	4.6±0.1	3.7±0.6	8±0.2
n_{pp}	0.63±0.32	0.50±0.30	0.56±0.06	0.34±0.06	0.17±0.84	0.2±0.5
$n_{\pi p}$	1.1±0.5	0.08±0.22	0.26±0.16	0.22±0.08	—	0.19±0.02

[a] Determined at 10 GeV/c for $\Delta(1236)$ and 15 GeV/c for the N^*'s.

$d\sigma/dt$ distribution which is assumed will effect the normalization; hence, the cross-sections at 30 GeV/c in Ref. [35] may be underestimated [37].

The process $p \to p\pi^+\pi^-$ has been studied in a number of experiments which give results which are in general agreement. The ABBCHLV collaboration has studied the reactions [38],

$$\pi^+p \to \pi^+(p\pi^+\pi^-) \text{ at } 16 \text{ GeV}/c \tag{6.3}$$

$$\pi^-p \to \pi^-(p\pi^+\pi^-) \text{ at } 16 \text{ GeV}/c \tag{6.4}$$

$$K^-p \to K^-(p\pi^+\pi^-) \text{ at } 10 \text{ GeV}/c \tag{6.5}$$

$$\pi^+p \to \pi^+(p\pi^+\pi^-) \text{ at } 8 \text{ GeV}/c \tag{6.6}$$

The combined effective mass of the $p\pi\pi$ system is given in Figure 33. It is clear from these data that the Δ^{++} plays a rather important role in these reactions. The authors report

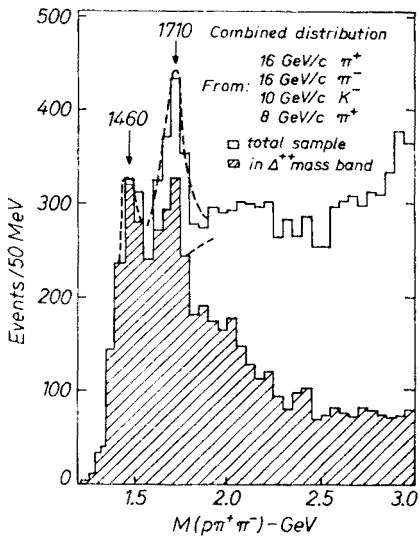

Fig. 33. The combined effective mass distribution of the $p\pi^+\pi^-$ system for the reactions 6.3 to 6.7. Shaded histogram are events in the Δ^{++} band. (Ref. [38])

that the best fit to the data is with Breit-Wigner forms at 1.47 GeV and 1.7 GeV with widths of 60 ± 20 and 57 ± 15 MeV, respectively. These enhancements are not observed in charge exchange reactions. This can be seen in Figures 25 (e–h).

The dependence of the production cross-sections on incident laboratory momentum is given in Figure 34. These experimenters claim that the 1470 and 1700 cross-sections can be described by $\sigma = C\,P_{\text{LAB}}^{-n}$, with $n \simeq 0.2\pm0.1$. The $d\sigma/dt'$ distributions give forward slopes of $\sim 15\,(\text{GeV}/c)^{-2}$ and $6\,(\text{GeV}/c)^{-2}$ for the 1.47 and 1.7 GeV regions, respectively. The $N^*(1700)$ seems to contain substantial $N^*(1470)\pi$ contribution, but it is not possible to make a clean separation.

Another interesting result is obtained from some of the same data (but a different combination of laboratories) by isolating the $T = 1/2$ and $T = 3/2$ contributions to

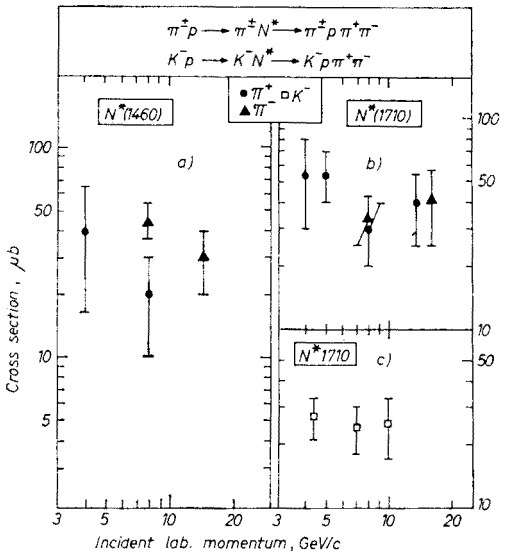

Fig. 34. Momentum dependence of production cross-section (Ref. [38])

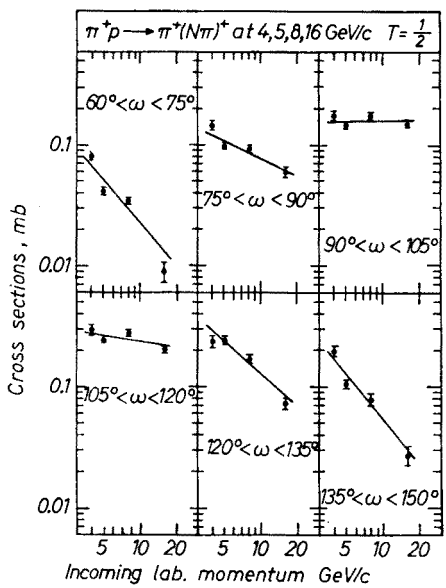

Fig. 35. The dependence on incoming laboratory momentum of the $T = 1/2$ contribution to the $\pi p \to N\pi\pi$ cross-section in different regions of the Van Hove plot (Ref. [39])

$\pi^{+}p \to \pi\pi N$ reactions [39]. They then combine this with a Van Hove phase space analysis. The results are presented in Figure 35. Here we see that in the region of the Van Hove plot where the $(N\pi)^{+}$ system goes "backwards" in the CMS the $T = 1/2$-cross-section is practically energy independent. It is also the only region where vacuum quantum number exchange is possible. At 16 GeV/c this region corresponds to approximately 70% of the

total $T = 1/2$ contribution. The $T = 3/2$ contribution falls like P_{LAB}^{-n} with $n > 1$ in all regions of the Van Hove plot.

The reaction $pp \to pp\pi^+\pi^-$ has been studied at several energies. In Figures 36a, b typical $p\pi^+\pi^-$ mass spectra obtained at 16 and 19 GeV/c are given [40, 41]. Enhancements in the region of 1.4 and 1.7 GeV are observed. Once again the important role of the Δ^{++} in the low $p\pi\pi$ effective masses is evident.

In the 19 GeV/c data the $d\sigma/dt$ distribution for $m(p\pi^+\pi^-) < 1.5$ GeV has a slope of 13 to 15 (GeV/c)$^{-2}$; the slope decreases with increasing mass to approximately 6 (GeV/c)$^{-2}$

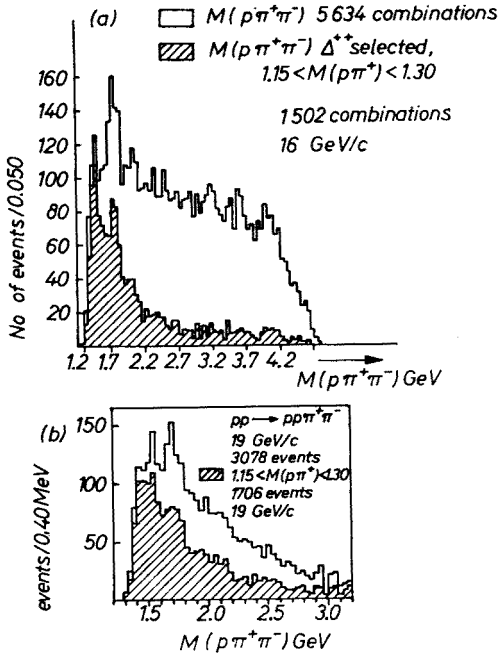

Fig. 36. Effective mass of $p\pi^+\pi^-$ system from the reaction $pp \to pp\pi^+\pi^-$. a) 16 GeV/c (Ref. [40]); b) 19 GeV/c (Ref. [41])

at $m(p\pi^+\pi^-) \simeq 1.7$ GeV. There is also evidence that the 1.45 GeV enhancement is not a pure angular momentum state, and its production is neither s- nor t-channel helicity conserving. The 1.7 GeV region is consistent with $J = 3/2$ or $5/2$ and t-channel helicity conservation.

In the 16 GeV/c experiment t-channel helicity is conserved in the production of $m(p\pi^+\pi^-) > 1.6$ GeV, while for $m(p\pi^+\pi^-) < 1.6$ GeV neither s- nor t-channel helicity is conserved. The spin parity analysis of the $p\pi^+\pi^-$ system gives $J \gtrsim 3/2$ over the whole mass region and $J \gtrsim 5/2$ contributions for masses greater than 1.8 GeV.

The SLAC 16 GeV/c π^+ and π^- data [18] has been analysed for nucleon dissociation in the reactions (6.3), (6.4) and $\pi^- p \to \pi^-(\pi^+ n)$. Events corresponding to reactions (6.3) and (6.4) were chosen by requiring that the two pions and the proton go backwards in the CMS. The effective mass spectra for high and low t' is shown in Figure 37. Although there

are only a few events there seems to be a trend; namely, the structure observed in the 1.7 GeV region is present only for large t' values in both $n\pi^+$ and $p\pi^+\pi^-$ final states. Within the statistical significance of this data, the low t' mass spectra have no structure. Note that a similar results was obtained in pion dissociation.

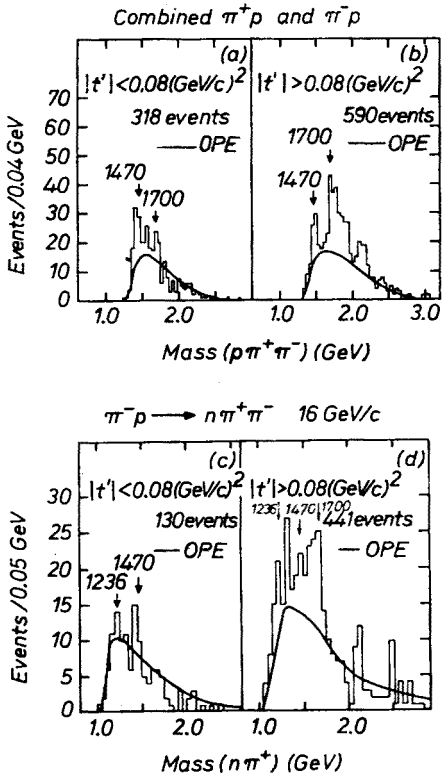

Fig. 37. Effective mass spectra of dissociated baryon obtained by the SLAC group at 16 GeV/c. (Ref. [18]) a) $p\pi^+\pi^-, t' < 0.08$ (GeV/c)^2; b) $p\pi^+\pi^-, t' > 0.08$ (GeV/c)^2; c) $n\pi^+$, $t' < 0.08$ (GeV/c)^2; d) $n\pi^+$, $t' > 0.08$ (GeV/c)^2

6.3. Summary

Missing mass experiments give evidence for production of $T = 1/2$ N^* resonances, which do not seem to be present in $n \to p\pi^-$ and $p \to p\pi^+\pi^-$ reactions at $t' \lesssim 0.08$ (GeV/c)^2. These experiments also suggest that the $d\sigma/dt'$ distributions for N^* production may "fall-off" at small t'; this might explain the absence of structure at small t'.

The $p\pi^+\pi^-$ mass spectra are dominated by $\Delta^{++}(1236)\pi^-$ threshold enhancements. The lower masses are mainly $J = 3/2$, while masses around 1.7 GeV have $J = 5/2$ states present.

The results obtained with nuclear targets agree with the small t' results of the SLAC experiment; the nuclear form factor clearly limits one to small t.

All experiments agree that s-channel helicity is not conserved. There is some indication particularly for the higher mass $p\pi\pi$ states that t-channel helicity is conserved.

7. *Discussion*

The data which have been discussed have certain similarities which are independent of the incident particle.

7.1. Comparison with elastic scattering

The similarities and differences between elastic scattering and the diffractive dissociation processes which have been discussed above are summarized in Table V. One can say with certainty that s-channel helicity is not conserved in these diffractive dissociation processes. The cross over effect seems to be a common feature. The low mass π

TABLE V

Similarities between elastic scattering and diffractive dissociation[a]

	$d\sigma/dt$		Cross--section	Cross over	Helicity conservation	
	Fwd. Peak	slope			s	t
Elastic	Yes		$\sim$ const.	Yes	Yes	
$\pi \to 3\pi$	Yes	$\sim$ E	$(\sim P_{\mathrm{LAB}}^{-0.5})$	A_1	No	NR
$\to 5\pi$	Yes	$\sim$ E	—	—	—	—
$K \to K\pi\pi$	Yes	$\sim$ E	NR	Q	No	NR
$N \to N^*$	No	< E	$(\sim P_{\mathrm{LAB}}^{-0.5})$	—	No	NR
$\to N\pi$	Yes	> E	NR	—	No	NR
$\to N\pi\pi$	Yes	> E	NR	—	No	NR

[a] ( ) indicates that result is uncertain; NR ≡ not resolved at this time; E ≡ elastic; — ≡ no information.

and K systems have a momentum transfer dependence which is very much like elastic scattering, but the nucleon does not seem to fit in this pattern. The dependence of cross-section on incident momentum is not well enough established to allow for a comparison.

It is clear that more experimental work is necessary. In particular: (*i*) The dependence of the production cross-section on incident momentum is not well known. (*ii*) The conservation or non-conservation of the t-channel helicity should be established. (*iii*) Nucleon dissociation must be studied for $t' \to 0$. (*iv*) A verification of observed cross over effects in Q and A_1 production and a study of this phenomena in nucleon dissociation is needed. (*v*) More data on $\pi \to 5\pi$ is needed.

7.2. General characteristics of three body diffractive processes

The dissociation of a hadron into three bodies has the property that the final state always consists of a pion and a resonance which decays into the incident particle and pion. This is shown symbolically in Eq. (7.1), where $\mathcal{N}$ represents the target and X the incident particle,

$$\begin{aligned} X+\mathcal{N} &\to Y+\mathcal{N} \\ &\quad \llcorner\!\to X^*+\pi \\ &\qquad \llcorner\!\to X+\pi. \end{aligned} \tag{7.1}$$

Such diffractive processes have the further properties:

(1) The observed M_Y mass distribution peaks near $M_{X^*}+M_\pi$.

(2) The momentum transfer to the nucleon is similar to that observed for Xp elastic scattering,

$$d\sigma/dt' \sim e^{At'}$$

where A depends on the target. (Note that nucleon dissociation has a greater slope than that found for pp elastic).

(3) For the case where X and X^* are bosons, the X^* system has been found to be predominantly in an s-state. This means that the diffractively produced bosons have unnatural parity $P = (-1)^{J+1}$.

(4) The cross-section is independent of energy.

(5) For the above data, the resonance X^* is in each case the lowest lying resonance which decays into the incident particle and the pion.

All of these points are summarized in Figure 38 and Table VI.

TABLE VI

Characteristics of three body diffractive processes

X	X^*'s	$(J^P_{X^*})$	$M_Y^{(1)}$ (GeV)	Name	$M_Y^{(2)}$ (GeV)	Name	$J^P_{Y_1}$ $J^P_{Y_2}$	σ_{YN}
π	(ϱ, f^0)	$(1^-, 2^+)$	0.95–1.2	A_1	1.5 –1.8	A_3	1^+ 2^-	~ 25 mb
K	(K^*_{890}, K^*_{1420})	$(1^-, 2^+)$	1.1–1.4	Q	1.65–1.95	L	1^+ 2^-	~ 20 mb
P	Δ_{1236}	$(3/2^+)$	1.3–1.6	?	—	—	? —	~ 40 mb

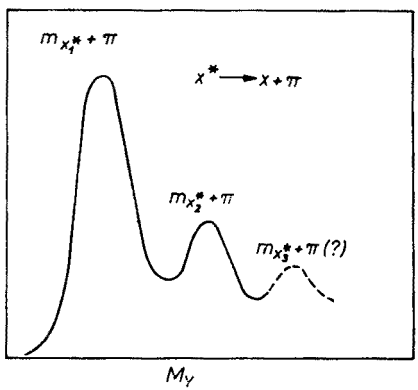

Fig. 38. Illustration of the importance of threshold effects in the dissociation of a hadron into three bodies

The observation that the three body diffractive dissociation mass spectrum looks as though it is the result of successive threshold effects which occur when the dissociating particle and a pion can resonate, suggests strongly that πX scattering is playing an important role. The five pion mass spectrum which gives an enhancement at the $\varrho\varrho\pi$ threshold supports this point of view. One might expect that the diffractive dissociation into higher multiplicities would give a series of threshold effects such as those sketched in Figure 39. A model which allows one to calculate such processes is the Drell-Hiida-Deck model.

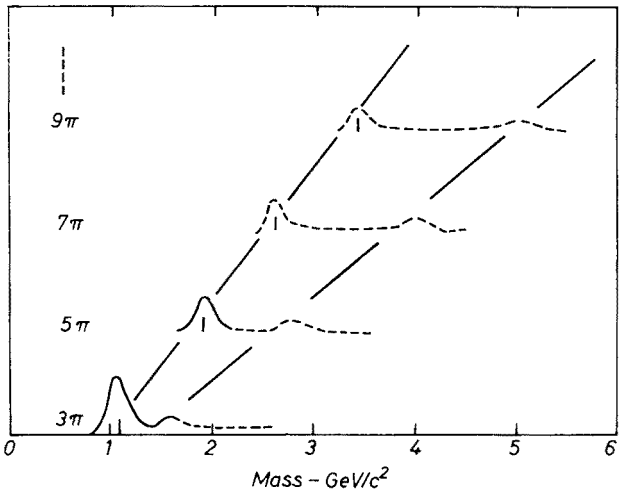

Fig. 39. Possible mass spectra for the various multiplicities into which a pion can dissociate if the dissociation mechanism involves $\varrho\varrho\ldots\pi$ and $f^0f^0\ldots\pi$ thresholds. The solid curves indicate observed enhancements

7.3. Drell-Hiida-Deck model

In this model the X threshold enhancement results from an off-mass-shell $X\pi$ interaction and π elastic scattering from the non-dissociating hadron (see Figure 40a). Because elastic scattering is strongly peaked in the forward direction and the pion propagator

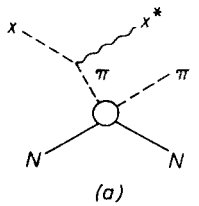

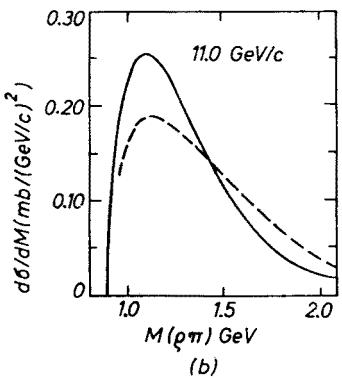

Fig. 40. a) Diffractive dissociation diagram; b) Comparison of $\varrho\pi$ invariant mass distributions calculated from the diagram of Figure 40a - - - Deck calculation (Ref. [42]), —— Reggeised calculation of Berger (Ref. [43])

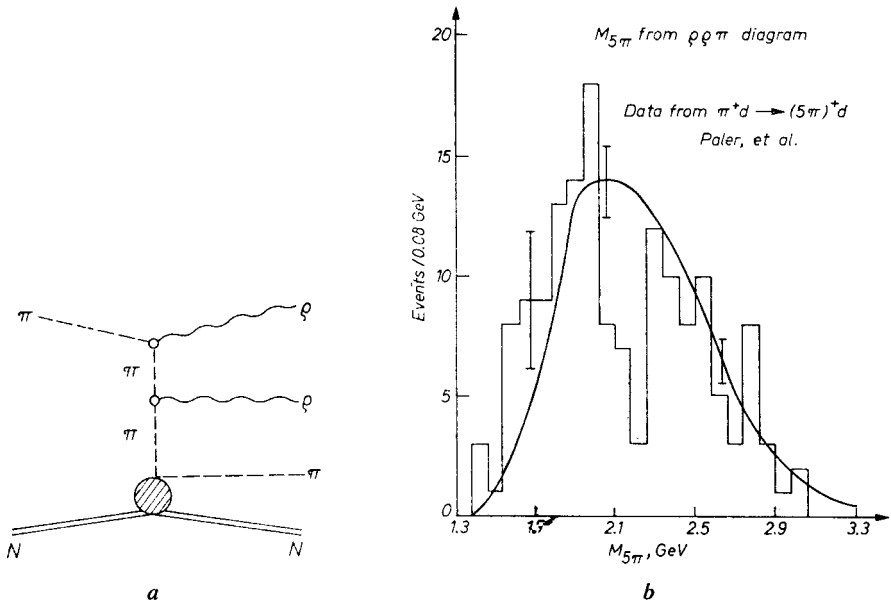

Fig. 41. a) Diffractive dissociation diagram for $\varrho\varrho\pi$ final states; b) $M(5\pi)$ distribution calculated from the diagram in Figure 41a using a reggeised pion propagator and elastic scattering. (The data are from Ref. [12])

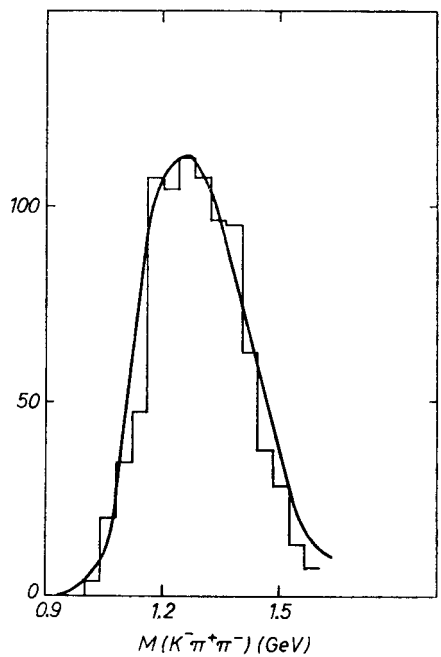

Fig. 42. Comparison of $K^{*0}\pi^-$ mass spectrum from Ref. [24] with a reggeised Deck calculation. Both the data and the calculated curve have the constraints $t' < 0.045$ (GeV/c)^2 and $0.8 < M(K^-\pi^+) < 1.0$ GeV

does not allow the X^* to have much transverse momentum, the resulting $X^*\pi$ mass spectrum peaks near threshold. The $\varrho\pi$ mass spectra obtained by Deck [42] using an OPE calculation and Berger [43] using a Reggeised pion propagator are shown in Figure 40b. A similar Reggeised calculation for the $\varrho\varrho\pi$ system gives the results shown in Figure 41b [44]. Note the agreement with data of Paler *et al.* The $K^*\pi$ mass spectra obtained from coherent production on nuclei is also reproduced by this double peripheral calculation (see Figure 42). Such calculations also reproduce the angular distributions of the $A_1 \to \varrho\pi$ and $Q \to K^*(890)\pi$ decays.

The cross over effect observed in Q production is difficult to explain as a Deck effect. A π propagator would give results in which the Q would have a greater slope than the $\bar{Q}$. Interchanging the roles of the $K^*(890)$ and the π in the calculation would give the correct cross over effect, but the mass spectrum one obtains is considerably broader than the experimentally observed Q.

There are difficulties in applying this calculation to pp interactions [45]. The large slope of the $d\sigma/dt$ distribution which is observed experimentally is not reproduced.

While many details are still uncertain, it seems probable that πX off-mass-shell scattering plays an important role in diffractive dissociation. The Drell-Hiida-Deck model is a way of calculating the contribution of πX scattering. It is almost certain that other processes are contributing to the observed phenomena.

8. New experimental techniques

In this section several new techniques which are being used to study diffractive dissociation are discussed.

8.1. "Triggered" bubble chambers

Because the bubble chamber is a 4π detector it is ideally suited for studying the dissociation of target nucleons.

In order to enhance the diffractive dissociation signal a Caltech-LBL collaboration [46] developed a triggering scheme where the mass recoiling against the fast forward particle is used to make a decision of whether or not to take a picture.

The experiment was carried out in a 14 GeV/c π^- beam using the SLAC 40 inch HBC; a total of 4×10^5 pictures were taken, which corresponds to approximately 7×10^6 expansions of the bubble chamber. Approximately 25% of the pictures contain good events; *i. e.*, events which can be used to study nucleon dissociation.

The apparatus, which consists of a single arm spectrometer downstream of the bubble chamber, is shown in Figure 43. Also shown are some typical parameters which are calculated on line. A momentum measurement in the spectrometer of the 14 GeV/c beam gives ± 75 MeV/c. By using the spectrometer information, the experimenters claim that a track can be located inside the bubble chamber to ± 1 mm. The calculated t-acceptance and missing mass acceptance of the spectrometer are given in Figures 44 and 45.

The Caltech-LBL group has proposed to do this experiment at 50 GeV/c at NAL using the Argonne 30 inch HBC [46].

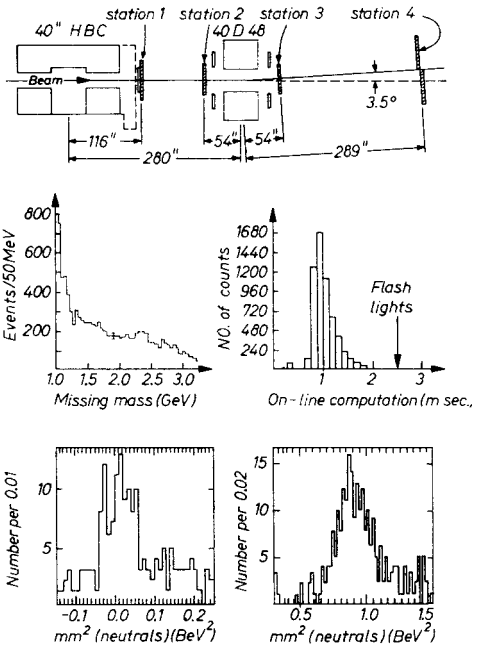

Fig. 43. Schematic of the SLAC "triggered" bubble chamber experiment. Also shown are some typical results calculated on line

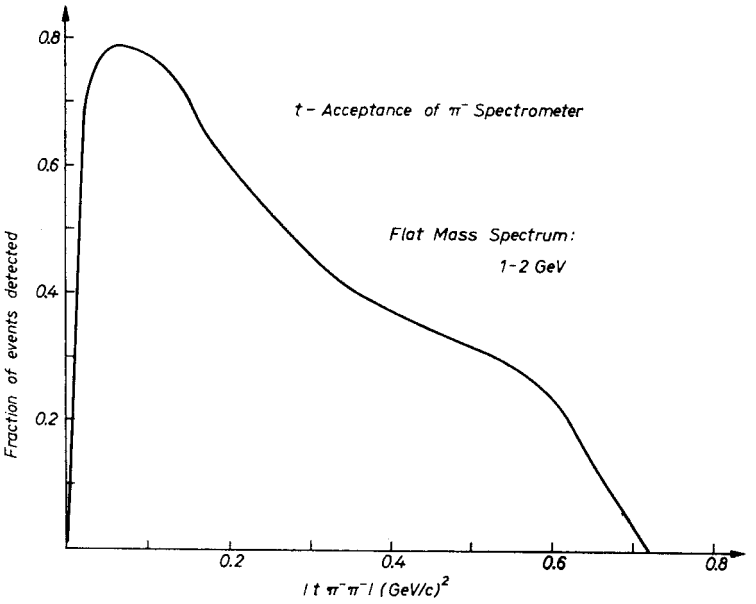

Fig. 44. Calculated t-acceptance of the Caltech-LBL spectrometer

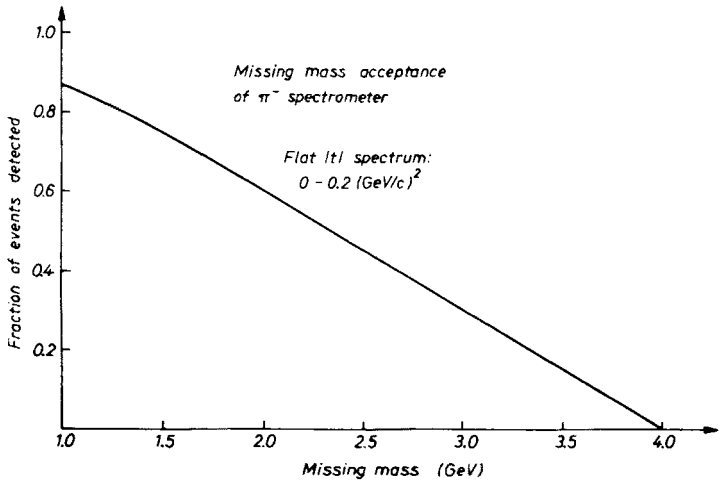

Fig. 45. Calculated missing mass acceptance of the Caltech-LBL spectrometer

8.2. Use of solid state detectors

The use of solid state detectors for the study of coherent production processes was first proposed by Lander *et al.* [47], who showed that it was possible to use a Si solid state detector as a target for elastic scattering of protons and to measure the recoiling nuclear momentum in the detector with sufficient accuracy to correlate it with the scattering angle.

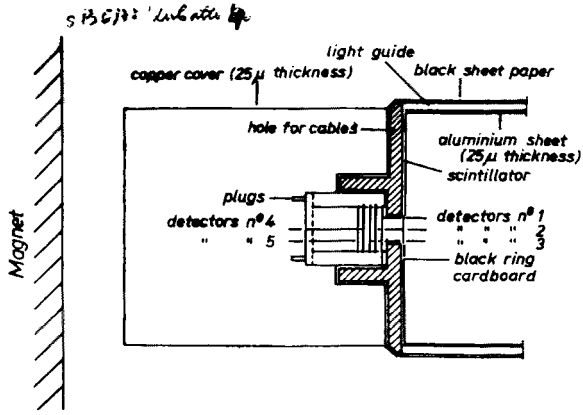

Fig. 46. Arrangement of Si SSD target in the anticoincidence counter of the CERN experiment of Ref. [11]

Later work showed that one could obtain fast signals of sufficient accuracy to allow triggering of optical spark chambers [48]. Bellini and co-workers at Milan have used a Si solid state detector target during the course of the CERN coherent production experiment (see Figure 46) [49]. The momentum transfer distribution which is obtained using the solid state detector is given in Figure 47. The main advantage of the solid state detector in such an experiment is to remove those incoherent events in which the nucleon recoils with insufficient momentum to be observed. There is indication that the background is substan-

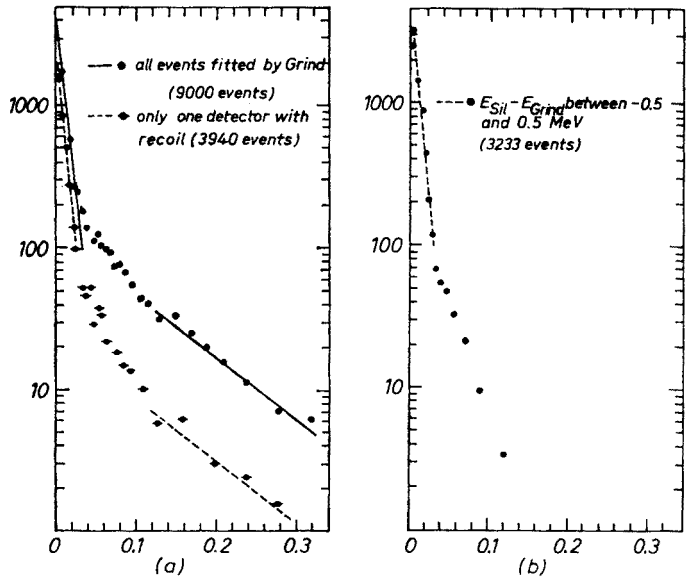

Fig. 47. a) t' distributions for all events and for events with the recoil in only one detector; b) t' distribution for $|E_{Sil}-E_{Grind}| < 0.05$ MeV and the recoil in only one detector

tially decreased when one combines the SSD information with that obtained by a kinematic fit which makes use of the momentum measurements of the fast tracks. The complete analysis of this experiment should be available soon.

8.3. The use of helium nuclei

Several proposals have been made for the use of helium nuclei. Helium has the advantage of being a relatively simple nucleus ($J = 0$, $T = 0$) for which all of its excited states are particle unstable. This gives one a better experimental handle in insuring that the nucleus is left in its ground state. It also makes simpler the determination of which state has been excited.

Experiments using helium nuclei have been proposed by Hertz and co-workers at CERN [50]. A diagram of their apparatus is shown in Figure 48. This involves strictly electronic techniques-wire chambers and plastic scintillators. The difficulty in using such apparatus is that in coherent processes the recoil momentum of the helium is usually less than 300 MeV/c. For example, a 250 MeV/c (350 MeV/c) He has a range of approximately 50 μ (100 μ) in mylar. In addition, if one wishes to study the coherent production of high mass states, he is obliged to measure recoiling helium nuclei which have a substantial q_L component; that is, a rather large component of momentum in the beam direction.

The use of a Helium streamer chamber as a target-detector, first proposed by the Seattle-Orsay collaboration, avoids most of the above difficulties [51]. The Seattle-Orsay experiment is approved to run in the M_1 beam of the meson laboratory at NAL. In this experiment, the streamer chamber gas is helium, which is also the target. Using an external trigger on the fast particles, the trajectory of the recoiling helium in a magnetic field is

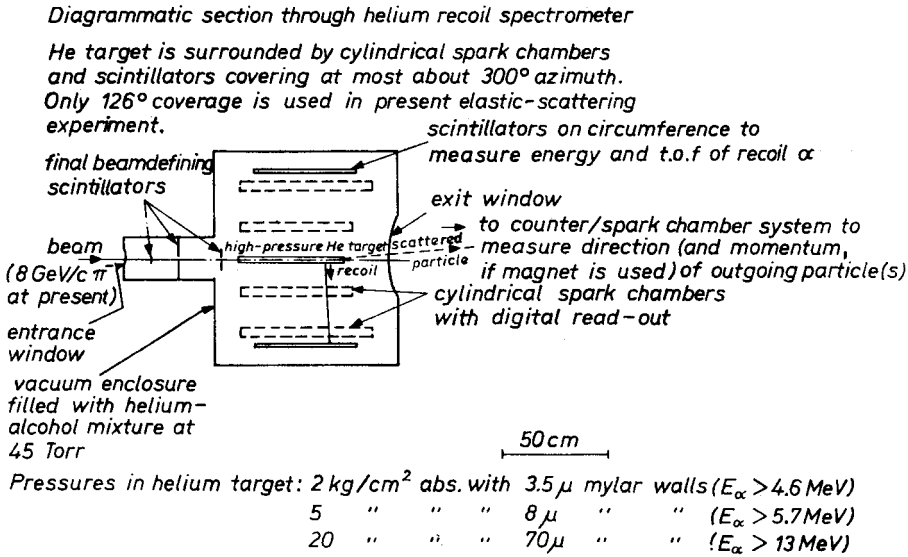

Fig. 48. Section of CERN Helium recoil spectrometer (Ref. [50])

photographed. For recoil tracks which are sufficiently long, the rate at which energy is lost allows one to separate ^{3}He from ^{4}He. In those cases where the helium stops in the chamber, the mass separation becomes quite good because both range and momentum are measured. It is also possible to have opening angle and momentum measurements of the fast pions, since these are also observed in the streamer chamber. Such a technique

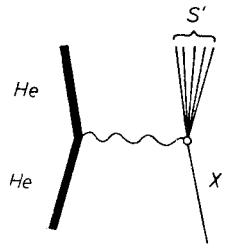

Fig. 49. X+He → He + anything, where X represents a hadron

seems to have considerable promise at high energy accelerators for the study of diffractive dissociation from He nuclei. These points are discussed in more detail below.

The first phase of the Seattle-Orsay experiment will concentrate on the inclusive diffractive dissociation reaction

$$\pi^- + \text{He} \rightarrow \text{He} + \text{anything} \tag{8.1}$$

Because He is identified in the final state, this experiment allows only vacuum quantum number exchange in the t-channel. The reaction is sketched in Figure 49. The mass s' of the multipion system which recoils against the nucleus, and the four momentum transfer

to the target can be determined from the longitudinal (q_L) and transverse (q_T) components of the He momentum, which is measured in the streamer chamber. Hence, the experiment measures $d\sigma/dt\, ds'$ which is a quantity of considerable theoretical interest [52].

The effectiveness of a streamer chamber in such experiment is best demonstrated by a plot of q_L *vs* q_T (Figure 50); $(s')^{1/2}$ and the efficiency of separating ^{4}He from ^{3}He are also given in Fig. 50 (s' is determined from q_L by Eq. (3.1)). The important experimental point is that the high mass states have recoils which are at small angles relative to the beam.

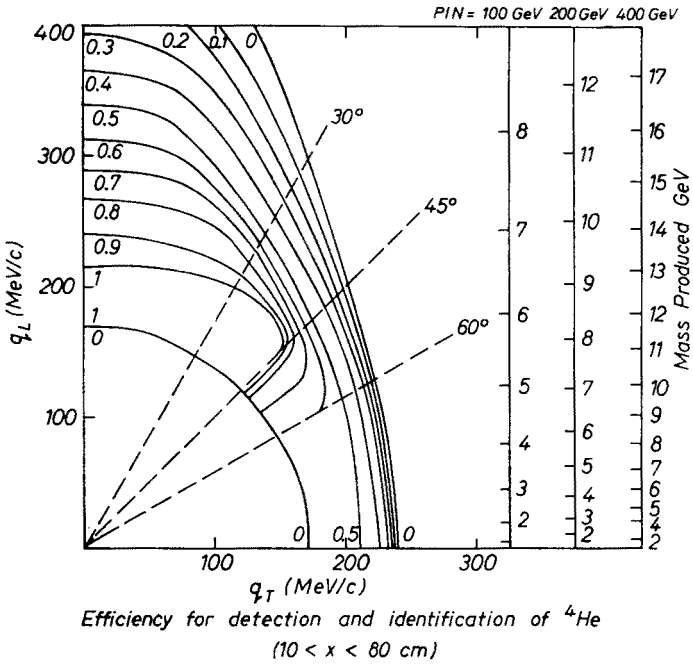

Fig. 50. Typical efficiency for detection and identification of ^{4}He, calculated for a volume of the chamber $10 < x < 80$ cm along beam

Recall that q is restricted by the nuclear form factor; hence, large q_L is correlated with small q_T. From Figure 50 it is obvious that the He streamer chamber is ideally suited for such measurements. A wire chamber detector would have difficulty in the forward direction (the reaction products all go forward).

In addition to measuring the momenta of the recoiling nuclei the momenta of the charged secondaries will be measured. However, the low magnetic field (12 KG) and short distances ($\sim$ 50 cm) over which measurements can be made will limit the accuracy of these measurements. A conservative estimate gives $\Delta P/P \approx 30\%$ at 10 GeV/c; however, this may be improved by using additional information from the trigger hodoscope, which is used to count the number of charged secondaries in each interaction.

For 1 mb of cross-section this experiment is expected to yield 10^4 events at each of two energies (typically 75 and 150 GeV/c). This estimate includes trigger efficiency and ^{4}He identification efficiency.

At each energy the elastic differential cross-section will be measured. This measurement is important since it will be useful in the normalization; it will also be important in separating the contribution of the helium vertex in reaction (8.1).

A summary of the relevant parameters of the experiment is given in Table VII.

TABLE VII

Typical parameters for NAL experiment 86A

Streamer Chamber	$100 \times 50 \times 30$ cm
Magnetic Field	12×10^3 Gauss over chamber volume
No of Pictures	10^6 (divided between two energies)
Incident energy	Typically 75 and 150 GeV
Error in missing mass (Δm)	50 MeV for $m = 3$ GeV
	100 MeV for $m = 2$ GeV
	200 MeV for $m = 1$ GeV
$\Delta P/P$ fast tracks in chamber	$\lesssim 30\%$ at 10 GeV/c
Evt./mb cross-section[a]	$\sim 10^4$ at each energy

[a] Includes trigger efficiency and ^{4}He identification.

I would like to thank Dr E. Obryk for having organized a very interesting and productive school. I also wish to thank the participants for many fruitful discussions. Finally, I wish to express my gratitude to Mrs E. Warchałowska, the secretary of the school, for her help. I would also like to thank Linda Shell for her help with the final typing.

REFERENCES

[1] I. Ya. Pomeranchuk, E. L. Feinberg, *Dokl. Akad. Nauk SSSR*, **93**, 439 (1953) and *Suppl. Nuovo Cimento*, **3**, 652 (1956); R. J. Glauber, *Phys. Rev.*, **99**, 1515 (1955); M. L. Good, W. D. Walker, *Phys. Rev.*, **120**, 1857 (1960); A. Białas, W. Czyż, A. Kotański, *Nuclear Phys.* **B46**, 109 (1972).

[2] V. Barger, F. Halzen, *Phys. Rev. Letters*, **28**, 194 (1972).

[3] K^-p M. Aderholz *et al.*, *Phys. Letters*, **24B**, 434 (1967); K^+p K. J. Foley *et al.*, *Phys. Rev. Letters*, **11**, 503 (1963). Figure taken from L. van Rossum, Proceedings of Topical Conference on High Energy Collisions of Hadrons, CERN, Geneva, Jan. 1968.

[4] Anzon *et al.*, *Phys. Letters*, **31B**, 241 (1970).

[5] A. Goldhaber, M. Goldhaber, *Preludes in Theoretical Physics*, (de Shalit *et al.*, eds) p. 313, North Holland, Amsterdam 1966.

[6] D. R. O. Morrison, *Phys. Rev.*, **165**, 1699 (1969).

[7] L. Van Hove, *Nuclear Phys.*, **B9**, 331 (1969).

[8] J. F. Allard *et al.*, *Phys. Letters*, **12**, 143 (1964); **19**, 431 (1965); *Nuovo Cimento*, **46**, 737 (1966).

[9] B. Daugeras *et al.*, *Phys. Letters*, **27B**, 332 (1968).

[10] N. S. Amaglobely *et al.*, Submitted to the 4th International Conference on High Energy and Nuclear Structure, Dubna, September 1971.

[11] C. Bemporad *et al.*, *Nuclear Phys.*, **B33**, 397 (1971).

[12] K. Paler *et al.*, *Phys. Rev. Letters*, **26**, 1675 (1971).

[13] W. Beusch, *Acta Phys. Polon.*, **B3**, 679 (1972).

[14] A. S. Goldhaber *et al.*, *Phys. Rev. Letters*, **22**, 802 (1969).

[15] R. Huson *et al.*, *Phys. Letters*, **28B**, 208 (1968).

[16] W. C. Harrison *et al.*, *Preprint* Lyman Laboratory of Physics, Harvard University, Cambridge, Mass.; G. W. Brandenberg *et al.*, *Nuclear Phys.*, **B16**., 287, 369 (1960).

[17] E. Bassler *et al.*, *Nuclear Phys.*, **B36**, 349 (1972).
[18] J. Ballam *et al.*, *Phys. Rev.*, **D4**, 1946 (1971).
[19] L. Van Hove, *Nucler Phys.* **B46**, 75 (1972).
[20] G. Ascoli *et al.*, *Phys. Rev. Letters*, **26**, 929 (1971).
[21] Aachen–Berlin–Bonn–CERN–Cracow–Heidelberg–London–Vienna Collaboration, *Phys. Letters*, **34B**, 160 (1971),.
[22] Aachen–Berlin–Bonn–CERN–Cracow–Heidelberg–London–Vienna Collaboration, CERN preprint to be published. I thank Dr Miettinen for bringing this result to my attention.
[23] G. Goldhaber, *Phys. Rev. Letters*, **19**, 976 (1967).
[24] A. M. Cnops *et al.*, *Phys. Rev. Letters*, **25**, 1132 (1970); B. Daugeras, *Thesis*, University of Paris, Orsay 1971; D. Fournier, *Thesis*, Univ. of Paris, Orsay 1970; S. Kahn, *Thesis*, Univ. of Calif. Berkeley 1972; Private communication D. Fournier.
[25] A. Firestone *et al.*, *Preprint* LBL-384, to be published in *Phys. Rev. D.*
[26] A. Firestone, The Q region of $K\pi\pi$ mass, in *Experimental Meson Spectroscopy*, ed. by C. Baltay and A. H. Rosenfeld, Columbia University Press, New York, p. 229 (1970).
[27] P. J. Davis *et al.*, to be published in *Phys. Rev.*, **D3**, June 1972.
[28] G. W. Brandenberg *et al.*, *Phys. Rev. Letters*, **28**, 932 (1972).
[29] Aachen–Berlin–CERN–London–Vienna Collaboration, *Nuclear Phys.*, **B35**, 61 (1971).
[30] For example: Aachen–Berlin–Bonn–CERN–Cracow–Heidelberg–Vienna Collaboration, *Phys. Letters*, **34B**, 160 (1971) favor t-channel helicity conservation, while F. Gard *et al.*, *Lett. Nuovo Cimento*, **2**, 305 (1971) find that neither s- nor t-channel helicity is conserved.
[31] M. J. Longo *et al.*, *Phys. Letters*, **36B**, 560 (1971).
[32] J. C. Vander Velde *et al.*, Univ. of Michigan *Preprint* UM HE 71–31.
[33] F. R. Huson *et al.*, *Nuclear Phys.*, **B8**, 391 (1968).
[34] E. W. Anderson *et al.*, *Phys. Rev. Letters*, **25**, 699 (1970).
[35] R. M. Edelstein *et al.*, *Phys. Rev.*, **D5**, 1073 (1972).
[36] E. W. Anderson *et al.*, *Phys. Rev. Letters*, **16**, 855 (1966).
[37] R. A. Carrigan, private communication.
[38] Aachen–Berlin–Bonn–CERN–Heidelberg–London–Vienna Collaboration, *Nuclear Phys.*, **B33**, 44 (1971).
[39] Aachen–Berlin–Bonn–CERN–Cracow collaboration, *Nuclear Phys.*, **B28**, 381 (1971).
[40] J. G. Rushbrooke *et al.*, *Nuclear Phys.*, **B35**, 1 (1971).
[41] H. Johnstad *et al.*, *Nuclear Phys.*, **B42**, 558 (1972).
[42] S. D. Drell, K. Hiida, *Phys. Rev. Letters*, **7**, 199 (1961); R. Deck, *Phys. Rev. Letters*, **13**, 169 (1964).
[43] E. L. Berger, *Phys. Rev.*, **166**, 1525 (1968).
[44] R. Harris *et al.*, *Bull. Amer. Phys. Soc.*, **17**, 612 (1972).
[45] H. I. Miettinen P. Pirilä, Rutherford Laboratory *Preprint* RPP/T/9. To be published.
[46] The experimenters involved are: A. Dzierba, W. Ford, R. Gomez, P. Oddone, C. Peck Caltech and R. Birge, R. Ely Jr., G. Gidal, D. Grether, W. Michael, W. Powel LBL (Also NAL proposal 157).
[47] R. L. Lander *et al.*, *Nuclear Instrum. Methods*, **42**, 262 (1966).
[48] R. L. Lander *et al.*, *Nuclear Instrum. Methods*, **67**, 173 (1969).
[49] G. Bellini *et al.*, in *Proceedings of the Topical Seminar on Interactions of Elementary Particles with Nuclei*, Trieste 1970, ed. G. Bellini, L. Bertocchi and S. Bonetti, p. 269.
[50] S. Dahlgren *et al.*, in *Proceedings of the Topical Seminar on Interactions of Elementary Particles witch Nuclei, ibid.* p. 261.
[51] NAL Proposal 86A, Seattle-Orsay collaboration. The experimenters involved are: P. L. Bastien, V. Cook, R. Gregg, A. Jonckheere, R. Kenyon, H. J. Lubatti, K. Moriyasu–Seattle; D. Fournier, P. Heusse, F. Jacquet, A. Lagarrigue, J. J. Veillet–Orsay.
[52] H. D. I. Abarbanel *et al.*, *Phys. Rev. Letters*, **26**, 937 (1971); C. E. DeTar *et al.*, *Phys. Rev. Letters*, **26**, 675 (1971).